Enhancing Resilience of FSO Networks to Adverse Weather Conditions

ILYA KALESNIKAU[1], **MICHAŁ PIÓRO**[2], (Senior Member, IEEE),
JACEK RAK[2], (Senior Member, IEEE), **HRISTO IVANOV**[3],
EMMA FITZGERALD[4], (Member, IEEE), **AND ERICH LEITGEB**[3], (Member, IEEE)

[1]Institute of Telecommunications, Warsaw University of Technology, 00-661 Warszawa, Poland
[2]Faculty of Electronics, Telecommunications and Informatics, Gdańsk University of Technology, 80-233 Gdańsk, Poland
[3]Institute of Microwave and Photonic Engineering, Technical University of Graz, 8010 Graz, Austria
[4]Department of Electrical and Information Technology, Lund University, 221 00 Lund, Sweden

Corresponding author: Jacek Rak (jrak@pg.edu.pl)

ABSTRACT Optical wireless networks realized by means of gigabit optical wireless communication (OWC) systems are becoming, in a variety of applications, an important alternative, or a complementary solution, to their fiber-based counterparts. However, performance of the OWC systems can be considerably degraded in periods of unfavorable weather conditions, such as heavy fog, which temporarily reduce the effective capacity of the network. In this paper, we focus on optical wireless mesh networks that use terrestrial links (called FSO – free-space optical – links) composed of several parallel full-duplex FSO systems, and present two complementary solutions that together provide a means to maximize network traffic performance in various weather conditions encountered during network operation. The first solution is a method for estimating the degradation of the effective FSO link capacity in adverse weather conditions such as fog, rain and snow (called the weather states in this paper). The second solution is an optimization model aiming at maximizing the network traffic throughput for a given list of weather states, derived from the conducted measurements. The model assumes the so-called affine flow thinning (AFT) traffic routing and protection mechanism capable of controlling the end-to-end traffic flows in response to fluctuations of capacity available on FSO links caused by changing weather conditions. The proposed link capacity modeling approach and the elaborated optimization model are verified through an exhaustive numerical study, illustrating the trade-off between the increase of traffic performance of the FSO networks and the corresponding cost of additional OWC systems.

INDEX TERMS Adverse weather conditions, affine flow thinning, FSO link capacity degradation, optical wireless communications, optimization, resilience, wireless mesh networks.

I. INTRODUCTION

Optical wireless communications (OWC) is a promising alternative (or a complementary solution) to optical fiber communications (OFC) [1]. In particular, OWC systems, based on light emitting diodes (LED) generating the optical signal at wavelengths in the 780–1600 nm range (encompassing visible light, infrared and ultraviolet [2]), are important for such applications as 5G communications and beyond [3],

The associate editor coordinating the review of this manuscript and approving it for publication was Hao Wang.

provisioning "last-mile" connectivity in metropolitan area networks [4], point-to-point and point-to-multipoint connections [5], and enabling connectivity in areas where fiber installation is hardly possible or costly [6].

Besides, over the last 15 years, optical wireless transmission systems have become critical to a variety of ground and aerial applications, in particular in relation to train, ship and airplane operation [7], [8].

In this paper, we consider still another, networking oriented application of the OWC systems, namely, optical wireless mesh networks (OWMN), relevant for example

for metropolitan areas [2], [9], [10] and cellular backhauling [11], [12]. In such networks links are composed of parallel full-duplex OWC systems of the range of several kilometers, referred to as free-space optical (FSO) systems, linking transceivers that are in line of sight. In metropolitan area networks (MAN) the transceivers can for example be installed on the roofs of high buildings. As compared to an alternative solution, that is wireless mesh networks using radio-frequency (RF) systems, the so-configured FSO networks have such important advantages (that stem from the usage of the FSO systems) as unlicensed spectrum, high full-duplex system capacity (of at least several Gbps) and robustness to electromagnetical interference [2]. Besides, components of FSO systems are characterized by low cost and power consumption as compared to RF equipment [13]. And, clearly, FSO systems do not require optical cables so their deployment cost is much lower than that of optical fiber-based systems.

In the related literature, FSO networks are often considered as a promising candidate solution to be widely used in the next decade 6G wireless backhaul networks due to their capacity by far exceeding that of RF systems [14], the possibility of dynamic rearrangement of FSO systems (reconfigurable topology to meet time-varying demands [15], or to adjust to changing adverse weather conditions [16]), cost-efficiency and scalability [17], as well as resource-efficiency and reliability [18]. Also, although currently the overall FSO market seems to be underdeveloped as compared to its potential, the usage of FSO systems is likely to be significantly boosted in the next few years [19].

It is worth noticing that a variety of FSO systems operating at a transmission rate of the order of 10 Gbps are already commercially available [2], [20], [21]. Also, research experiments have shown a remarkable potential of the FSO systems in increasing nominal transmission rates, e.g., up to 1.72 Tbps for distances of over 10 km (see [22], [23]), or even up to 13.16 Tbps over a distance of 10.45 km (achieved in 2018 by DLR and ADVA) – *https://www.adva.com/en/newsroom/press-releases/20180510-dlr-and-adva-set-new-world-record-for-optical-free-space-data-transmission*.

Although solutions to issues concerning, e.g., advanced modulation and coding [24], [25], or multiple access [26] have been provided, the adverse weather conditions characteristic to the lowest part of the atmosphere up to 10 km above the Earth sphere (i.e., the troposphere also called the weather sphere) can still pose severe problems to FSO communications. Indeed, apart from many challenges to resilient communications highlighted in [13], [27] including

1) atmospheric turbulence (also called scintillation [22]) responsible for increased bit error rate (BER) and decreased signal-to-noise ratio (SNR) due to random changes of the atmospheric refractive index; atmospheric turbulence typically decreases with the altitude (except for weather inversion periods when the opposite behaviour can occur) [28],

2) a proper pointing, positioning and tracking of signal (mechanical alignment issues)

as already mentioned, FSO communications can often be substantially affected by the adverse weather conditions such as fog, clouds and snow [10], leading to partial or even complete unavailability of multiple FSO links at a time. Although the impact of weather conditions is mostly temporal, the frequency of their occurrence implies the need to pay special attention to the mitigation of their effect on the performance of FSO communications.

Concerning multihop transmission in OWMNs, the atmospheric attenuation caused by weather conditions can be observed in multiple locations at a time along the routing path. Generally, this attenuation is low during clear days but can increase during periods of adverse weather conditions [29], [30]. Among all weather events, fog has been found responsible for the most significant degradation of FSO link capacity. Especially during periods of thick fog, a remarkable Mie scattering causing deflection of a part of the light beam from the receiver can be observed, as the size of water droplets (between 1 and 20 μm) is similar to the size of infrared wavelengths [27].

The impact of fog on FSO link capacity has been found to depend also on the fog type. Maritime fog has been verified to cause the highest attenuation of even several hundred dB/km (similar to clouds). The impact of continental fog was found to be lower – about 100 dB/km. Besides, continental fog is more stable than the maritime one [22]. It is worth noting here that Mie scattering can also occur in the areas of clouds [22] and, therefore, affect space-to-ground communications. However, since in this paper we consider only terrestrial FSO systems operating below clouds, the impact of clouds is beyond the scope of this paper.

Concerning other weather conditions such as rain and snow, their influence on the performance of FSO systems is relatively low. In particular, higher robustness of FSO systems to rain, as compared to fog, is due to the radius of rain-drops being commonly greater than 100 μm (which is visibly larger than the FSO wavelengths [31], [32]). As a result, rain can typically cause only geometrical scattering with a minimal influence over the optical laser energy [33]. Typical signal attenuation due to rain is, therefore, marginal (about 3 dB/km [5]) and can be meaningful only under severe rain [7]. The effect of snow is also not significant and positioned between the impact of light rain and moderate fog [7].

As wireless systems based on RF transmission are robust to fog conditions, a hybrid RF/FSO architecture has been investigated in several research papers (see, e.g., [34], [35]). Indeed, these two technologies can be often regarded as complementary since the weather events affecting RF and FSO systems are diverse (FSO systems are vulnerable to fog, snow and clouds, while RF transmission is sensitive to rain [7]). However, the nominal capacity of FSO systems is typically far greater than that of RF ones [7]. Therefore, in such hybrid configurations, RF links can be used, for example, to provide parallel transmission of only part of the traffic (for instance of

high-priority). Another application of RF links could be for control plane purposes (RF links acting as control plane links while FSO systems being used for data transmission). As the RF technology is costly (due to exclusive licensing of most of the RF sub-bands [7]), and since RF links installed parallel to FSO systems cannot assure full recovery of all the affected FSO flows, such a hybrid architecture is not considered in our paper.

In this paper, we aim at investigating the impact of fog, rain and snow on the performance of operating FSO networks, and at elaborating an optimization model for reconfiguring the location of the FSO transmission systems to maximize the (network) traffic throughput in all (nominal and adverse) weather conditions that can be expected during network operation. Furthermore, when considering atmospheric conditions (such as fog and rain), we neglect atmospheric turbulence. This is assumed for three reasons:

1) realistic consideration of atmospheric turbulence would require reliable measurement results, which were not available in the databases we could access
2) some FSO architectures (such as Multiple Input Single Output (MISO) [22]) are robust to atmospheric turbulence
3) considering atmospheric turbulence effects in the optimization model presented in Section IV would lead to losses in its effectiveness.

More precisely, our investigations can be summarized as follows.

1) Development of a methodology for determining the influence of adverse weather conditions on the degradation of the FSO system capacity. In effect, we obtain formulas which determine the fraction (called link availability coefficient) of the maximal capacity (expressed in Gbps) that is available on an FSO system between two given locations, based on the weather records that specify the parameters of fog, rain and snow conditions. With such formulas we are then able to calculate the availability coefficients for all links and all states in a given network inside a certain area (like the Paris metropolitan area analyzed in the numerical part of the paper) for which the weather records, typically for each hour of the year, are available. In such records, the area is represented by a grid of measurement points separated by a fixed distance, and the weather conditions observed in a given hour at each node are characterized by fog type and density (visibility), as well as rain/snow intensity (precipitation rate) impacting the overall visibility. Based on that, a list of representative weather states characterized by link availability coefficients can be prepared for an FSO network of interest.
2) Development of an optimization model for maximizing the traffic throughput taking into account all weather states from a given (realistic) list of states prepared as described above. For this, we assume a traffic

routing and protection mechanism called affine flow thinning (AFT) capable of on-line controlling the end-to-end traffic flows in response to fluctuations of link capacity caused by changing weather conditions. In effect, the AFT parameters necessary for the effective day-to-day operation of the network can be set.

As compared to earlier works, the originality of the presented approach consists of two major elements. First, the methodology for determining the FSO link availability coefficients for adverse weather conditions is novel and more adequate for links with the length of the order of kilometers than the previous modeling proposals of this kind. Second, the optimization model for the FSO systems reconfiguration, combined with an appropriate traffic flow routing and protection mechanism and the max-min fairness objective for traffic throughput that is supposed to be realized in different weather states, is a far-reaching extension of the previous optimization models for FSO networks.

The remaining part of the paper is organized as follows. First, in Section II, we present the works related to modelling FSO link capacity available under adverse weather and summarize the state-of-the-art in optimization models suitable for traffic routing and protection. Then, in Section III, we introduce our model for determining the degradation of the FSO link capacity due to unfavorable weather conditions, while in Section IV we describe our optimization approach to maximize the network traffic throughput in scenarios of reduced link capacity. A numerical study verifying the proposed optimization procedure for FSO network traffic protection under adverse weather conditions (based on the real weather data collected for the Paris metropolitan area) is presented in Section V. Section VI concludes the paper.

II. RELATED WORKS

Considerations of this paper belong to the field of resilient network design that takes into account not only the nominal condition of network operation but also scenarios when the network capacity is not fully available. Below, we will briefly discuss the work in this field related to two fundamental problems dealt with in our paper: modeling of FSO transmission systems availability in adverse weather conditions, and network optimization models taking into account the limited availability of the capacity of network links.

A. FSO LINK AVAILABILITY UNDER ADVERSE WEATHER CONDITIONS

Performance of an FSO system strictly depends on the type of the selected technology, commonly IM/DD-based (Intensity Modulation/Direct Detection) [36]. Design of terrestrial FSO systems resilient to the background noise/attenuation involves non-conventional solutions, where apart from amplitude, also phase modulation is utilized. This is for example the case for FSO systems considered in [36]. In such terrestrial systems using the optical-intensity modulation techniques, FSO transmission can be characterized by the IM/DD AWGN

(additive white Gaussian noise) channel model. In most cases, the intensity-modulated information is transmitted in discrete periods that transform the terrestrial channel into a discrete-time one. For example, in an urban areas considered in Section V, FSO terrestrial systems realizing direct transmission within distances of several kilometers are exposed to adverse weather conditions – mostly to fog (the Mie scattering) and also partly rain and snow often leading to severe attenuation of the optical signal, and thus also limiting the available link capacity. In general, atmospheric turbulence also causes fading, worsening the quality of the received optical signal. Nevertheless, the used hereby multiple input FSO systems [22] aim to significantly mitigate the effect of turbulence which is neglected due to the need for additional specific weather data for the area of Paris. Furthermore, the evaluation of its influence is the subject of further work.

In general, the Mie theory is a complex but useful tool to evaluate interaction between water droplets in the air and the optical signal. In particular, assessment of the impact of fog on FSO transmission is possible, for example through applying the superposition principle for a given distribution of fog particle size and the Mie theory [37]. However, weather stations that measure the weather-related parameters in an urban FSO network (such as temperature, density, humidity, and the empirical visibility) are usually not equipped with particle size analyzers [37].

Because of the complexity of the Mie analytical approach, empirical models for calculating the Mie scattering attenuation based on the notion of visibility (denoted by V) are often applied. The most important models include those of Kim, of Kruse and of Al Naboulsi [22], [38] for accurate evaluation of optical attenuation, which, apart from the weather-related factors, also depends on physical FSO link characteristics such as wavelength and distance.

A comparison of the models by Kim, Kruse and Al Naboulsi is presented in [38]. As stated in [22], the Kruse model proposed for the visibility range reaching over 50 km is mainly designed for a dense haze and its precision for fog with $V \leq 1$ km is low. To address this issue, the Kim and Al Naboulsi empirical models should be considered. In particular, the Al Naboulsi model is suitable for the wavelength range between 0.69 and 1.55 mm and provides formulas dedicated to maritime and continental fog. The disadvantage of this model is the 1 km limit on the visibility parameter. Similarly to the Kruse model, the Kim model covers the entire visibility range and additionally provides high accuracy for $V \leq 1$ km. A characteristic feature of the Kim model is that if $V \leq 0.5$ km, the fog attenuation is non-wavelength dependent [33]. Therefore, the Kim model is often considered in the literature as the most accurate approach for determining fog attenuation.

It should be mentioned here that the most general method for evaluation of channel capacity is based on Shannon information theory [39], and the efforts in finding solutions to the problem of evaluating the information capacity of the intensity-modulated FSO signals are presented in many research papers summarized for example in [40]. However, methods of a straightforward calculation of the FSO system capacity expressed in bits per second [bps] are hardly available. This is because the IM/DD AWGN FSO channel is characterized by peak, average and non-negativity constraints on the parameters specifying a given random variable describing the input of a communication channel (related to the optical power of a light source), which requires a different approach [40].

Hence since the Shannon theory cannot be applied directly for FSO systems, only the upper and lower bounds on the available system capacity can be determined. In particular, the upper bound on the FSO channel capacity can be calculated using a dual expression for the channel capacity [41], or sphere-packing [42]. For the case of continuous random variables used for input characterization, the lower bound can be determined, using for example the expressions discussed in [40]. Moreover, the case of the lower bound of the channel capacity is examined for the capacity-approaching discrete distributions. While, in general, the throughput is expressed in bits per symbol [40], when considering the time domain, metrics expressed in bits per second (bps) are well-suited for the empirical analysis of FSO systems.

The complexity of the problem of determining accurate upper and lower capacity bounds calls for introducing an approximation method for determining the channel capacity based on signal-to-noise ratio (SNR). As the maximum data rates of commercially available FSO systems are expressed in Gbps (e.g., 10 Gbps), derivation of the available link capacity must be done without a direct use of the Shannon theory. In fact, an important contribution of this paper is introduction of an approximation method to evaluate the available link capacity for IM/DD AWGN channels depending on the bit error ratio (BER) expected for a given SNR [24].

A detailed derivation of the available FSO system capacity based on the normalized SNR [43] and the corresponding BER is introduced in Section III-C. The BER parameter is of major importance for evaluating the available FSO system capacity, as it allows for consideration of the influence of all types of noise (for example background noise) and the adverse atmospheric effects on the operation of optical wireless links. Although theoretical solutions for obtaining BER values (applied in the current paper in terms of the on-off keying (OOK) modulation) of various IM/DD FSO systems are widely used and well defined in the literature [24], a reasonable accuracy of BER estimation can be obtained only if real measurement data are used.

Finally, we would like to mention that a method for evaluating the fraction of the FSO link capacity lost because of an unfavorable weather condition (with respect to the maximal capacity realized in a good weather condition) is considered in papers [44]–[46]. The method assumes that link capacity is controlled by means of adjusting the modulation and coding scheme (MCS) used in order to make it appropriate for the current channel condition. Thus, when bad weather (like fog, rain or snow) is observed, an appropriate MCS, allowing for

an increased SNR threshold (but decreased bitrate), is applied at the transmitter. In the method, a simple characterization of the weather condition affecting a given link, namely the worse of the two conditions observed at its end nodes is assumed for all points along the link. A detailed description of the method can be found in [47].

B. OPTIMIZATION MODELS

In general, the optimization part of this paper is devoted to traffic protection in networks, the links of which are subject to frequent capacity degradation. In particular, it applies to optical wireless networks (like OWMNs), where the links are exposed to unfavorable weather conditions (e.g., fog) that weaken the optical signals delivered to the receivers and thus reduce the actual throughput provided by the links.

As such, our investigations deal with the multi-state optimization of multicommodity flow networks – an important area of operations research.

However, although the research achievements in the above-mentioned area include a wide set of optimization models for a variety of network applications (see [48]–[50]), they do not encompass the model introduced in this paper. Our proposal examines the case where an operational network, designed to handle traffic in clear weather, is expected to efficiently protect the traffic against adverse weather conditions described by means of a list containing *link availability states* corresponding to typical situations characterized by subsets of links that lose a fraction of their normal (maximal) capacity realized when the transmitted optical signal is not disrupted. To capture these features, the following opportunities are included in our model.

1) To make room for traffic protection under the considered conditions of reduced network capacity, it is assumed that the operating FSO transmission systems can be rearranged. Also, a set of additional systems can be installed within some extra budget.
2) A special traffic routing and protection (TRP) mechanism (a particular case of the so-called *affine flow thinning* (AFT) mechanism) that ensures a quick response to link capacity fluctuations is considered when the rearrangement and extension of link capacity is optimized.
3) The traffic volumes realized for individual demands in the reduced-capacity states are maximized in a fair manner.

These items, although clearly advantageous for the considered purpose, have virtually not been considered in the literature. The reasons are as follows.

1) The models considered so far are focused mainly on joint link capacity and routing optimization in order to minimize the total cost of the links assuming that the entire traffic specified in the traffic matrix is restored in the states (called failure states in this context) other than the normal state.

2) Traffic routing and protection/restoration mechanisms considered in optimization are either hardly implementable but traffic-efficient (unrestricted or restricted flow restoration, or link restoration), or vice versa (path diversity, hot stand-by).
3) Almost all models assume that in the failure states the capacity of a link is either totally unavailable or fully available. However, even such states (sometimes referred to as *shared-risk link groups*—SRLG [51]) are considered less commonly than the single-link failure states, where only one link can be unavailable at a time.
4) Even when the requirement of 100% traffic protection is relaxed, it is assumed that fractions of the demand traffic volumes to be realized in the considered states are predefined.

A detailed discussion of these issues can be found in the monograph [50], the doctoral dissertation [48] and the article [52].

Let us now summarize the works that share common elements with the optimization approach presented in this paper. Like our model, the model presented in [53] (see also [54]) examines a network with given link capacities and traffic flows and optimizes the amount of capacity to be released on each link and used as protection capacity by the link protection mechanism. For this, the demand volumes specified in the traffic matrix must be decreased, and this is done using the max-min fairness concept. The main difference as compared to our approach is that in [53], [54] only single-link failures are assumed and that the assumed protection mechanism is different.

Another relevant work is presented in [55], where a joint link capacity and routing optimization problem is studied in the context of microwave links, whose capacity is dependent on the modulation and coding scheme and the channel condition. The approach uses chance-constrained programming with independent random variables characterizing link availability (our approach uses an explicit description of link availability states). The problem assumes static routing and realization (with a given probability) of a given traffic matrix in all states, thus considerably simplifying the problem.

It is also worthwhile to mention that among the traffic routing and protection/restoration strategies considered in the literature, only unrestricted reconfiguration (also called *global rerouting* – GR) is applicable in the partial multiple link failure context considered in our model. This particular mechanism restores the demands traffic by establishing path-flows from scratch in the surviving link capacity. This feature makes GR virtually impractical due to excessive end-to-end flow rerouting (and other reasons, such as erroneous flow control decisions in the unforeseen weather states). On the other hand, from the theoretical point of view GR is the most efficient traffic restoration mechanism we can think of and because of that can be useful for testing the efficiency of other mechanisms, including TRP. An application of GR to a joint link capacity and routing optimization problem relevant

to the link availability state characterization used in our model is studied in [45].

The two main elements of our optimization approach are the use of the max-min fairness (MMF) principle for traffic throughput maximization and the assumed routing and protection mechanism (TRP).

As far as the MMF principle and its applications in multi-commodity network design are concerned, our investigations are based on the material presented in [50] (Chapter 8) and, in more detail, in [54], [56]. The assumed TRP mechanism is a special case of the so-called *affine flow thinning* (AFT) which is a variant of the general concept called *flow thinning* (FT) originally introduced in [57].

FT is an active TRP mechanism, where the end-to-end traffic demands are equipped with dedicated logical tunnels (for example MPLS tunnels) whose maximal capacities are subject to thinning to respond to the fluctuations of the currently available link capacities. In consequence, the instantaneous traffic realized between the end nodes of the demands must adjust to the current total capacity available on its dedicated tunnels. FT can be viewed as an extension (to multiple partial link failure scenarios) of a path diversity traffic protection mechanism called *demand-wise shared protection* (DWSP) proposed in [58] (see also [52], [59], [60]) that assumes multiple total link failures. In DWSP, traffic flows using currently unavailable links are deleted, and the remaining path flows must be sufficient to meet the (possibly reduced) traffic volumes given in the traffic matrix.

Let us note that FT is also related to a specific mechanism called *elastic rerouting* [61].

The affine versions of FT are based on the idea introduced in [62]. In AFT, the capacity of each tunnel is thinned according to a tunnel-dependent flow thinning function – an affine function whose arguments are the link availability coefficients (recall that for a given link, such a coefficient is the fraction of the maximal link capacity available in a given link availability state). This makes AFT different from the FT solution, where the tunnels can be thinned in an unconstrained manner. Due to that, AFT becomes feasible for potential implementations, and also applicable to the states not foreseen when optimizing the parameters of affine thinning functions. For a detailed description of AFT and its implementation issues the reader is referred to [57], [63]–[66].

Finally, let us observe that the FSO network optimization model introduced and studied in this paper is based on rigid problem formulations and exact solution algorithms involving linear and mixed-integer programming methodology underlying modern solvers. However, other approaches can be thought of, first of all those based on heuristic methods that allow for extending the range of tractable problems at the expense of limited capability of delivering globally optimal solutions and, for that matter, also of approximate solutions with a given gap. This kind of approach to FSO (and other networks') optimization can be found, for example, in [67].

III. EVALUATING THE DEGRADATION OF FSO LINK CAPACITY IN ADVERSE WEATHER CONDITIONS

This section presents our approach to estimate the link availability coefficients α. In particular, the derivation of the formula for this parameter is given in Section III-B, while in Section III-C we describe our method used in this paper to estimate the current capacity of FSO systems due to the considered weather conditions, namely fog, rain and snow.

A. THE CONSIDERED FSO SYSTEM

The advances in FSO technology provide a wide spectrum of commercially available products that are installed in various urban access networks as well as backhaul and last-mile communication links [11], and can be considered for WMNs as well. For reasons of simplicity, the implemented FSO transceivers are assumed in our paper to be properly aligned and are based on Multiple Input Single Output (MISO) architecture being a slightly improved version of Single Input Single Output (SISO) architecture serving normally as a benchmark for performance analyses [26]. In particular, this type of architecture involving multiple transmitters (i.e., ≥ 4), allows for significant mitigation of atmospheric turbulence [22]. Moreover, the utilized FSO transceivers are based on Intensity Modulation/Direct Detection (IM/DD) scheme consisting of internally modulated laser source with On/Off keying (OOK) modulation as well as a receiver supporting direct detection of the incident optical intensity [68]. Those types of transceivers are easily realized even based on small form-factor pluggable (SFP) devices that offer high data rates of 10 Gbps. The basic concept of the utilized transceivers is provided in Fig. 1. Furthermore, a general set of parameters for FSO systems operating at 10 Gbps (at distances between 2.38 km and 12.65 km in the topology analyzed in our paper) discussed, e.g., in [30], [69]–[71], are presented in Table 1.
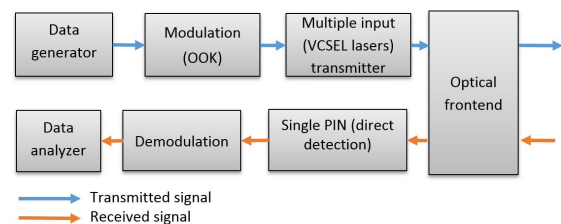
FIGURE 1. A basic structure of the utilized FSO transceiver.

In particular, the used transceivers within the considered urban FSO network are selected to operate at 10 Gbps The operating wavelength is 1550 nm and the normalized electrical SNR is assumed to be a fixed value of 45 dB independent of the link distance. In order to achieve such performance for all considered FSO scenarios, each system architecture is designed in accordance with the FSO link distance. Considering the different lengths of FSO link (i.e., 2.38–12.65 km), an example for a 10 km FSO link operating at 10 Gbps is given in [70] and [71]. Moreover, a shorter link of 2.7 km implemented in the architecture considered by us in this

TABLE 1. Assumed FSO system parameters.

FSO parameter		Min	Max
Link distance		2.38 km	12.65 km
Number of transmitters		≥ 4	
Wavelength		1550 nm	
Transmitter	Tx power	6 dBm	15 dBm
	Tx optics (diameter)	6.5 mm	6.5 mm
	Beam divergence angle	0.279 mrad	0.1 mrad
Receiver	Rx power	-16 dBm	-28 dBm
	Rx optics (diameter)	50 mm	100 mm
	Sensitivity	-16 dBm	-30 dBm
Other parameters	Data rate	10 Gbps	
	Tx core diameter (SMF)	8.2 μm	
	Rx core diameter (MMF)	105 μm	

paper (Fig. 1) is provided in [30], [70]. As discussed in [30], [69]–[71], the parameters of all FSO systems should be carefully tuned. In particular, the FSO transmitters implement vertical-cavity surface-emitting laser (VCSEL) operating at 1550 nm and supporting typical FSO optical power of 4–15 dBm. Having in mind the used MISO architecture with larger number of separate transmitters, the accumulated optical power is boosted and eye-safety regulations should also be considered. While in general, VCSELs are low-power lasers, much higher power can be generated with VCSEL arrays at the expense of beam quality. Moreover, distributed feedback laser (DFB) is also a well-suited alternative operating in the range between 0.8 μm and 2.8 μm with a few tens of milliwatts [26]. In general, the used PIN photodetector, converting the received optical signal into electronic signal is characterized by a threshold between -30 dBm and –16 dBm for a maximum BER of 10^{-8}. In case of larger distances, also avalanche photodiode (APD) can be applied. Both APD and PIN utilize germanium or indium gallium arsenide (InGaAs) substrates when longer wavelengths up to roughly 1.7 μm are needed.

The applied MISO architecture leads to considerably facilitated arrangement with single frontend optics at the receivers as well as multiple optics in the transmitter part. In particular, the divergence angle of the transmitters is between 0.1 and 0.3 mrad and the frontend lens of the receiver is featured with 50–100 mm diameter [71].

In the proposed architecture, the normalized electrical SNR is 45 dB (for all considered link distances of 2.38 km–12.65 km), which value can be enhanced with changes of the transmitter and receiver technologies in parallel to adjusting the frontend optics characterized by divergence angle and lens diameter. However, using such a predefined SNR value in our paper allows considering a simplified model not requiring a detailed FSO link budget.

B. FORMULAS FOR FSO SYSTEM CAPACITY UNDER ADVERSE WEATHER CONDITIONS

In general, the capacity available on a given FSO system changes over time as it depends on the time-varying BER, which, in turn, follows from the instantaneous SNR, which is, in turn, characterized by the given level of signal

attenuation (A). As presented in [38] and explained in the introduction of this paper, the overall instantaneous attenuation A of an FSO system due to atmospheric effects including fog, rain and snow is composed of three components as shown in the following formula

$$A = A^f + A^r + A^s, \qquad (1)$$

where A^f, A^r, A^s denote attenuation (in [dB]) caused by fog, rain and snow, respectively, observed at the receiver of a given system. Note that in a given weather state, only one of these three attenuation components can be greater than 0, which means that fog, rain and snow exclude each other. A way of calculating these values is described in Section III-C.

Attenuation A observed at the receiver of a given FSO system is a major factor impacting the SNR measured in the electrical domain. Following [43], the normalized variant of SNR (that is SNR_n with its values expressed in [dB]) can be specified as:

$$SNR_n = SNR_t - SNR_{th} - 2A \qquad (2)$$

where

- SNR_{th} is the SNR threshold value defined for scenarios without the presence of free-space atmospheric effects given by formula (3) being a function of photodetector responsivity ρ, the noise intensity variance σ^2 of the AWGN channel model, and the required minimum optical power P_{th} for clear-air conditions [43]:

$$SNR_{th} = \frac{(\rho \times P_{th})^2}{\sigma^2} \qquad (3)$$

- SNR_t is the SNR at the target (receiver) node for the scenario of geometrical scattering (rain and snow) and the Mie scattering (fog) attenuation expressed by the formula:

$$SNR_t = \frac{(\rho \times P_{th})^2}{\sigma^2}(P \times A)^2 = SNR_{th} \times (P \times A)^2 \quad (4)$$

where P is the power required for an acceptable quality of transmission in the presence of atmospheric effects (therefore $P > P_{th}$), while the other parameters in formula (4) have the same meaning as in formulas (2) and (3). Similarly to [43], the current analysis relies on a simplified approach, where the quality of transmission is characterized by means of SNR. In effect, the characterization based on optical power P is omitted.

Since formula (2) uses the logarithmic scale in [dB], subtraction of SNR_{th} from SNR_t allows for confining the analysis only to the atmospheric effects (without a detailed consideration of the FSO system performance). Following the fact that FSO systems are characterized by the target electrical SNR_t of up to 60 dB [7], the difference between SNR_t and SNR_{th} for adverse weather conditions can be substituted by a constant value, e.g., of 45 dB in the electrical domain which corresponds to the value 22.5 dB in the optical domain extracted from figure 1 presented in [72] in the case

TABLE 2. BER performance of a typical terrestrial IM/DD FSO system based on OOK modulation concerning the Mie scattering (fog) from [30].

Parameter	Month of the year											
	January	February	March	April	May	June	July	August	Sept.	October	Nov.	Dec.
BER	4.4E-11	1E-12	1.7E-11	6.6E-14	2.5E-11	6.5E-12	4.4E-13	2.3E-13	7.9E-12	2.3E-11	1.7E-11	1.7E-11
Capacity [%]	83.06%	99.88%	90.65%	100%	99.97%	99.38%	99.96%	99.97%	97.23%	94.05%	81.07%	79.52%

$BER = 10^{-12}$ and OOK modulation. (The relation of the SNR values in optical and electrical domains is explained in [73].) In general, the selected value of the electrical SNR equal to 45 dB corresponds to the highest operational SNR of a standard IM/DD system operating with OOK. Therefore, formula (2) can be rewritten as follows:

$$SNR_n = 45 - 2A \text{ [dB]}. \quad (5)$$

The value of SNR_n has, in turn, a direct impact on the bit error ratio (BER) of an FSO system. As BER is expressed in a non-logarithmic scale, the transformation of the normalized SNR_n in [dB] into its SNR'_n counterpart in the non-logarithmic scale [73] is applied as follows.

$$SNR'_n = 10^{SNR_n/10}. \quad (6)$$

Assuming

- the AWGN channel model
- the fixed pulse detection threshold of 0.5 (a standard assumption for binary transmission channels for equally distributed symbols with probability 0.5),

the value of BER can be obtained for most of the commercial FSO systems implementing the IM/DD technique combined with on-off keying – non-return to zero (OOK-NRZ) modulation [73] using the formula:

$$BER = \frac{1}{2}\text{erfc}\left(\frac{\sqrt{SNR'_n}}{2\sqrt{2}}\right), \quad (7)$$

where erfc is the error function (i.e., the Gauss error function).

Based on the concept described in [68] for the packet error rate, the capacity c of a given link for a given BER is calculated as follows:

$$c = \hat{c} \times (1 - BER)^{\frac{k}{\log_2 M}}, \quad (8)$$

where $\hat{c}$ is the nominal capacity of an FSO system (data rate), k is the number of bits of the transmitted packet, and M is the order of Pulse Position Modulation (where $M = 2$ for the OOK modulation assumed in this paper). A typical FSO packet size k for the Ethernet protocol is 512 bits (64 bytes), but it can reach up to 12,176 bits (1522 bytes). The analysis presented in this paper is done for $k = 512$ bits.

Finally, the link availability coefficient $\alpha(A)$ referring to the degradation of the capacity of an FSO system is defined as given in the following formula.

$$\alpha(A) = \frac{c}{\hat{c}} = (1 - BER)^{\frac{k}{\log_2 M}}. \quad (9)$$

Fig. 2 presents the values of BER (calculated for a realistic value of the electrical SNR = 45 dB) and the related normalized link capacity (parameter $\alpha = c/\hat{c}$) as a function of atmospheric optical attenuation.
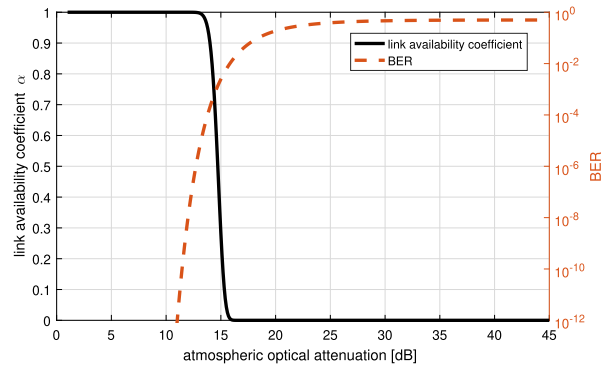

FIGURE 2. Link availability coefficient α and BER as a function of the overall atmospheric optical attenuation ratio.

Table 2 presents an example of the average monthly values of BER and the available link capacity for an IM/DD system operating under typical continental European weather conditions in Austria from [30].

C. CALCULATION OF ATTENUATION ALONG A LINK

Suppose that a set of M measurement points (called M-points) representing weather stations is available in the considered network area. The network area is represented by a rectangle in the first quadrant of the coordinate system with one of the vertices placed at point (0, 0). These M-points will be indexed with $m = 1, 2, \ldots, M$ and identified by the coordinates $x(m), y(m)$. We assume that the M-points keep track of the basic parameters characterizing the fog, rain and snow (and, for that matter, that these parameters are stored in a database). The parameters in question are visibility (V for fog, in [km]), and precipitation rate (φ for rain and ψ for snow, both in [mm/h]).

Moreover, we assume that for any point (x, y) of the considered rectangle we can reasonably estimate (by means of some calculation procedure) the values of parameters V, φ, ψ observed at (x, y) corresponding to the values of these parameters measured at the M-points (clearly, when (x, y) happens to coincide with an M-point, then the estimation must provide the actual values). Note here that for the considered estimations there is software available that finds the approximation function $F(x, y)$, the values of which coincide with the set of values determined for a given set of points $\{(x(m), y(m)) : m = 1, 2, \ldots, M\}$ in the given rectangle. For example, in [74], [75] three such approximations, one non-continuous (nearest-point approximation) and two

continuous (piece-wise linear approximation and piece-wise cubic approximation) can be found.

Let us now consider a given FSO link, denoted by AB, linking nodes A and B with respective coordinates $x(A)$, $y(A)$ and $x(B)$, $y(B)$. For convenience, AB will be represented by interval $[0, D]$ on the horizontal axis, where D is the line-of-sight distance between A and B, i.e., the Euclidean distance

$$D = \sqrt{(x(A) - x(B))^2 + (y(A) - y(B))^2}.$$

This is done by first translating and rotating plane (x, y) so that point A of interval $[A, B]$ is moved to point $(0, 0)$ and point B to $(D, 0)$. Then each value $z \in [0, D]$ represents the corresponding point $Z(z)$ in $[A, B]$ in the original plane, and the values of $V(z)$, $\varphi(z)$, $\psi(z)$ are calculated by the assumed approximation procedure for point $Z(z)$.

The above considerations are illustrated in Figs. 3 and 4. The considered link AB (of length $D = 10.26$ km) is depicted in Fig. 3, and its horizontal representation (obtained by translation/rotation) in the lower part of Fig. 4. The figures show the case when the nearest point approximation of the measurements from the M-points is assumed and the visibility parameter V is analyzed. The circles depicted in colors show the locations of the six M-points (note that there are in total 168 M-points in the considered rectangle) which are actually used in the nearest-point approximation for the points in interval $[A, B]$. The following visibility values $V(k)$, $k = 1, 2, \ldots, 6$, are assumed for those M-points: 3, 2, 2, 1, 1, 2.
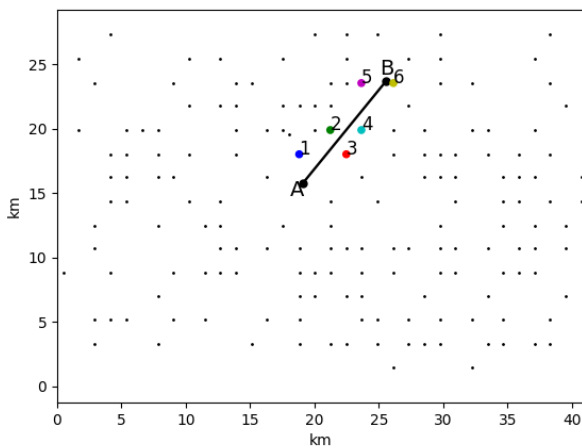
FIGURE 3. The network rectangle, M-points, link AB and its nearest M-points.

In the lower part of Fig. 4 the interval $[0, D]$ on the horizontal axis is divided into colored subintervals, where the subinterval of a given color represents the points in the corresponding subinterval of $[A, B]$ for which the M-point of the same color is the nearest one. Finally, in the upper part of Fig. 4, we plot the approximation of the visibility function $V(z)$ characterizing link AB for the above-listed visibility values observed at the colored M-points. This piece-wise constant function is represented in the upper part of Fig. 4 by brown segments.
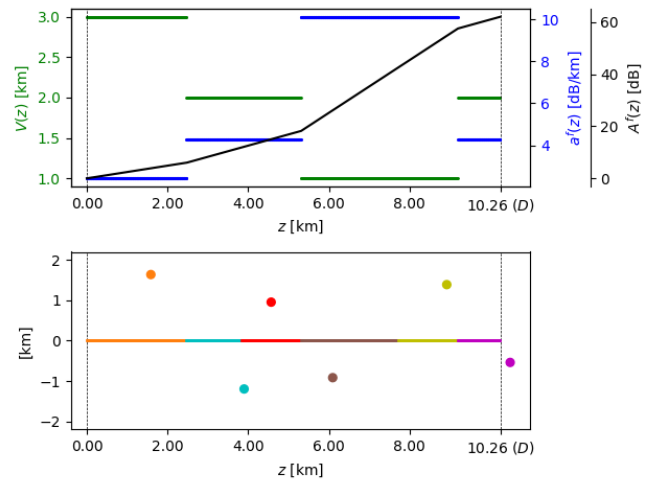
FIGURE 4. Representation of link AB and its nearest M-points in the translated/rotated plane (lower part) and the visibility function $V(z)$, the corresponding attenuation rate function $a^f(z)$ and the attenuation function $A^f(z)$ for link AB (upper part).

Now we proceed to the main issue, i.e., the way of calculating the attenuation (expressed in [dB]) experienced by the optical signal sent from node A to node B. We will first describe such a calculation for a foggy weather state; in this case the attenuation in question will be denoted by A^f. We will come back to the rainy or snowy weather state cases afterwards. (In fact, fog has been reported to be responsible for the most significant attenuation, due to the Mie scattering, (see [22]) among all the weather factors that can affect optical wireless transmission.)

Basic for the calculation of A^f is the following formula that expresses the attenuation rate $a^f(z)$ at a given point z along the link by means of the visibility $V(z)$ observed at this point:

$$a^f(z) = \frac{10 \log_{10}(\frac{1}{\tau})}{V(z)} \left(\frac{\lambda_0}{\lambda_1} \right)^{-q(V(z))}. \tag{10}$$

The above empirical formula for the fog-related attenuation rate expressed in [dB/km] follows from the considerations discussed in [24], [33], [76].

Following [68], the visibility $V(z)$ shown in Fig. 4 is defined as 2% or 5% (i.e. the visual contrast threshold τ) of the atmospheric transmission distance, for which only black objects on the horizon can be detected. While 5% is the proper value of the visual contrast threshold τ for aeronautical purposes, in our case the proper value of τ is equal to 2%. Moreover, the wavelength of the transmitted optical signal λ_0 used due to eye-safety regulations is 1550 nm, and the reference wavelength λ_1 is equal to 550 nm.

The last parameter in formula (10), i.e., the value of the quantity $q(V)$ in the exponent depends on the visibility V

(expressed in [km]) in the following way:

$$q(V) = \begin{cases} 1.3, & \text{if } 6 \le V \le 50 \\ 0.16\,V + 0.34, & \text{if } 1 \le V < 6 \\ V - 0.5, & \text{if } 0.5 \le V < 1 \\ 0, & \text{if } 0 < V < 0.5. \end{cases} \quad (11)$$

For the considered example, the values $a^f(z)$, $0 \le z \le D$, of the attenuation rates along link AB are calculated for the values determined by the $V(z)$ and plotted in the upper part of Fig. 4.

Finally, let $A^f(z)$ denote the attenuation (expressed in [dB]) of the optical signal sent (from point A) along link AB observed at any given point $Z(z)$ lying on link AB ($z \in [0, D]$). Then, by the definition of attenuation we get:

$$A^f(z) = \int_0^z a^f(t)\,dt. \quad (12)$$

Observe that the attenuation we are looking for, i.e., the attenuation observed at node B experienced by the optical signal sent from node A, is given by $A^f(D)$.

Clearly, for the piece-wise constant visibility function $V(z)$ resulting from the nearest-point approximation (depicted in Fig. 4), calculation of the value of the integral in (12) is straightforward, as illustrated in the upper part Fig. 4. However, in the case of more sophisticated (and more accurate) approximations, like piece-wise linear or piece-wise cubic approximations, calculation of the visibility for a given point (x, y) on the plane is done by means of some algorithm (because the formula specifying the approximation function $V(x, y)$ is not available), and therefore computation of $A^f(z)$ specified in (12) must be done by some approximate numerical method. For example, in order to calculate the attenuation at point B, we can divide the interval $[0, D]$ into n subintervals of equal length (equal to $\frac{D}{n}$), determine the visibilities $V(z)$ and attenuation rates $a^f(z)$ at the end of these subintervals and compute the sum

$$A^f(D) = \frac{D}{n} \sum_{i=1}^{n} a^f(i), \quad (13)$$

where $a^f(i)$ is the average of the values of the attenuation rates at the two end points of subinterval number i.

Concerning rainy and snowy weather, since droplets of water are substantially larger than λ_0, the resulting geometrical scattering has typically a negligible effect on attenuation (<3 dB/km), and its effect at optical SNR greater than 20 dB on link capacity is insignificant. In practice, it means that only FSO links longer than 2-3 km can become noticeably affected by rain and snow. The respective empirically derived formulas for a^r and a^s (expressed in [dB/km]) described in [26], [38] are as follows:

$$a^r(z) = 1.29 \times \varphi(z)^{0.64} \quad (14)$$
$$a^s(z) = (0.000102 \times \lambda_0 \times 10^{-9} + 3.79) \times \psi(z)^{0.72}, \quad (15)$$

where $\varphi(z)$ and $\psi(z)$ express the precipitation rates (in [mm/h]) observed at point $Z(z)$ respectively for rain and snow.

Clearly, the corresponding attenuations $A^r(z)$ and $A^s(z)$ are computed by means of formula (12).

IV. OPTIMIZING NETWORK TRAFFIC THROUGHPUT IN THE STATES OF REDUCED LINK AVAILABILITY

In this section, we will present an optimization approach based on mixed-linear programming (MIP) formulations, which aims to solve the problem of protecting traffic in a network with varying link availability.

The problem is as follows. Let us consider an operating network that implements a given traffic matrix in a normal state where all links (and nodes, for that matter) are fully available. However, the network is subject to external conditions (such as changing weather) that affect the capacity currently available on the links, i.e., they reduce the capacity of a subset of links below their nominal (maximum) level. Thus, in order to protect the traffic in the states of reduced link capacity (called degradation states), the operator should be able to reschedule the traffic flows upon a given state, so that the maximum traffic throughput is achieved and, what is important, accomplish this in a fair way, i.e., ensuring that the traffic between all individual node pairs is evenly reduced.

To achieve this goal, two basic decisions must be made. One is a protection/routing mechanism applied for traffic flow reallocation, and second what measure of fairness in traffic restoration to select. The solution we consider below assumes, respectively, the affine flow thinning (AFT) mechanism [57], [64] and the max-min fairness (MMF) measure [50], [54], [56]. The proposed optimization approach is composed of two main phases: preprocessing of path lists and link capacity, and an iterative phase of MMF optimization.

A. NETWORK DESCRIPTION

The notation related to the network model and to the optimization problems considered in this paper is summarized in Table 3. Generally speaking, the network is modeled by means of an undirected graph $\mathcal{G} = (\mathcal{V}, \mathcal{E}, \mathcal{D})$, where $\mathcal{V}$ is the set of nodes, $\mathcal{E}$ is the set of undirected links, and $\mathcal{D}$ is the set of undirected (traffic) demands. The number of nodes is denoted by V (i.e., $V = |\mathcal{V}|$), the number of links by E (i.e., $E = |\mathcal{E}|$), and the number of demands by D (i.e., $D = |\mathcal{D}|$). Thus, each link $e \in \mathcal{E}$ represents some unordered pair of nodes $\{v, w\}$, and so does each demand $d \in \mathcal{D}$. The capacity of link e is specified by a given integer number $c(e)$ expressing the number of transmission systems (FSO systems in our case) installed on this link. Each such transmission system has a fixed capacity of M traffic demand units (e.g., 10 Gbps). Thus, the total bandwidth realized on a link is equal to $Mc(e)$. This bandwidth is realized in the normal network operation state denoted by 0. In fact, in the optimization model used in this paper, we will assume that $M = 10$ Gbps.

The traffic demand volumes to be realized (i.e., carried) in the normal state are denoted by $h(d)$, $d \in \mathcal{D}$. Each demand volume $h(d)$ is realized by means of path-flows that use an admissible set of paths $\mathcal{P}(d, 0)$ between the end nodes of a demand d, selected from the set of all simple paths, where

TABLE 3. Notation.

PARAMETERS	DESCRIPTION
$\mathcal{V}$	set of nodes $v \in \mathcal{V}$
$\mathcal{E}$	set of (undirected) links $e \in \mathcal{E}$
$\mathcal{D}$	set of (undirected) traffic demands $d \in \mathcal{D}$
$\mathcal{S}$	set of link availability states $s \in \mathcal{S}$
$\mathcal{Q}$	set of demand-state pairs ($\mathcal{Q} = \{(d,s) : d \in \mathcal{D}(s), s \in \mathcal{S}$)
$\mathcal{P}(d,0)$	set of paths $p \in \mathcal{P}(d,0)$ assigned to demand $d \in \mathcal{D}$
$\mathcal{P}(d,s)$	set of paths $p \in \mathcal{P}(d,0)$, $d \in \mathcal{D}$, available in state $s \in \mathcal{S}$
$\mathcal{R}(d,e,0)$	set of those paths $p \in \mathcal{P}(d,0)$ that traverse link e
$\mathcal{R}(d,e,s)$	set of those paths $p \in \mathcal{R}(d,e,0)$ that are available in state $s \in \mathcal{S}$
$\mathcal{E}(d,p)$	set of links composing path $p \in \mathcal{P}(d,0)$, $d \in \mathcal{D}$
$\mathcal{D}(s)$	set of demands $d \in \mathcal{D}$ with at least one path $p \in \mathcal{P}(d,0)$ available in state $s \in \mathcal{S}$
$f(d,p,0)$	nominal path-flow, $d \in \mathcal{D}$, $p \in \mathcal{P}(d,0)$
$f(d,p,s)$	state path-flow, $s \in \mathcal{S}$, $d \in \mathcal{D}$, $p \in \mathcal{P}(d,0)$
$z(d,p,e)$	coefficients of the affine thinning formulae, $e \in \mathcal{E}$, $d \in \mathcal{D}$, $p \in \mathcal{P}(d,0)$
$\xi(e)$	unit capacity cost, $e \in \mathcal{E}$
$c(e)$	link capacity, $e \in \mathcal{E}$ (equal to the number of the FSO systems installed on the link when $\xi(e) = 1$)
$\alpha(e,s)$	link availability coefficients, $e \in \mathcal{E}$, $s \in \mathcal{S}$; $0 \le \alpha(e,s) \le 1$
$\beta(e,s)$	link degradation coefficients, $e \in \mathcal{E}$, $s \in \mathcal{S}$; $\beta(e,s) = 1 - \alpha(e,s)$
$h(d)$	traffic demand volume, $d \in \mathcal{D}$
$w(s)$	state weight, $s \in \mathcal{S}$
$F(s)$	proportion of the total capacity of network links available in $s \in \mathcal{S}$ with respect to the total maximum link capacity
$T(s)$	traffic reduction factor, $T(s) = w(s)F(s)$
$h(d,s)$	state-dependent (reduced) demand traffic volume, $h(d,s) = T(s)h(d)$
B	upper-bound on network cost (budget)

VARIABLES	DESCRIPTION
x_{dp}^0	nominal path-flow, $d \in \mathcal{D}$, $p \in \mathcal{P}(d,0)$
x_{dp}^s	state path-flow, $s \in \mathcal{S}$, $d \in \mathcal{D}$, $p \in \mathcal{P}(d,0)$
y_e^0	link capacity, $e \in \mathcal{E}$
z_{dp}^e	coefficients of the affine thinning formulae, $e \in \mathcal{E}$, $d \in \mathcal{D}$, $p \in \mathcal{P}(d,0)$
t	traffic reduction factor

the set of all such paths is denoted by $\widehat{\mathcal{P}}(d,0)$. Recall that a path $p \in \widehat{\mathcal{P}}(d,0)$ is simple if it does not contain loops and thus can be described by means of the set of links $\mathcal{E}(d,p)$ it traverses.

As the network is subject to unfavorable weather conditions, its links are subject to capacity degradation. In effect, when the network experiences a weather state $s \in \mathcal{S}$ (where $\mathcal{S}$ is the set of the considered states and $S = |\mathcal{S}|$ is its cardinality), the bandwidth realized by the transmission systems installed on some of the links is in general degraded. This is reflected by given *link availability coefficients* $\alpha(e,s)$ (where $0 \le \alpha(e,s) \le 1$, $e \in \mathcal{E}, s \in \mathcal{S}$), meaning that the actual bandwidth on link e in state s is in general decreased and equal to $\alpha(e,s)Mc(e)$. In the following, we will also use the notion of *link degradation coefficient* $\beta(e,s)$, where $\beta(e,s) = 1 - \alpha(e,s)$, $e \in \mathcal{E}, s \in \mathcal{S}$.

Note that when $\alpha(e,s) = 0$ then link e is unavailable in state s, so the set of links available in state s (i.e., the links with $\alpha(e,s) > 0$), denoted by $\mathcal{E}(s)$, can be a proper subset of $\mathcal{E}$. (In the following we will use a symmetrical notion $\mathcal{S}(e)$ – the set of states where link e is available.) In effect, some paths from the sets $\widehat{\mathcal{P}}(d,0)$ may become unavailable (the set of paths from $\widehat{\mathcal{P}}(d,0)$ that are available in state s will be denoted by $\widehat{\mathcal{P}}(d,s)$). Moreover, the network graph can become disconnected and split into disjoint components. In this case, the demands with the end nodes in different components cannot be realized at all. (In the following, the set

of the demands that can be realized, i.e., the demands having the end nodes in the same component will be denoted by $\mathcal{D}(s)$.) In general, when the network is in state s we do not require that the entire demand volumes $h(d)$ are realized; actually, we admit a decreased volume, $h(d,s)$, to be realized. These (decreased) carried volumes are realized by means of path-flows using allowable sets of paths, $\mathcal{P}(d,s)$, $d \in \mathcal{D}(s)$, where $\mathcal{P}(d,s) \subseteq \widehat{\mathcal{P}}(d,s)$.

In the optimization problem formulations considered in this paper, we will use several kinds of variables. In particular, when the link capacities are optimized, then they are expressed by variables $\boldsymbol{y}^0 = (y_e^0, e \in \mathcal{E})$. Path-flows, in turn, will be denoted by $\boldsymbol{x}^0 = (x_{dp}^0, d \in \mathcal{D}, p \in \mathcal{P}(d,0))$ (flows in the normal state) and by $\boldsymbol{x}^s = (x_{dp}^s : d \in \mathcal{D}(s), p \in \mathcal{P}(d,s))$ (flows in state $s \in \mathcal{S}$).

Please note that in the following the variables will be considered as continuous, unless otherwise specified. We will also use a notational convention that places the indices in brackets in the case of constant parameters (like $c(e), f(d,p,s), z(d,p,e)$), while in the case of the corresponding variables the indices will appear as subscripts or superscripts (like $y_e^0, x_{dp}^s, z_{dp}^e$).

B. PATH LISTS AND LINK CAPACITY PREPROCESSING
Consider a network with a given link capacity vector $\boldsymbol{c} = (c(e), e \in \mathcal{E})$ that is dimensioned to carry a given traffic matrix represented by vector $\boldsymbol{h} = (h(d), d \in \mathcal{D})$ of demand

traffic volumes. This means that the traffic volume $h(d)$ for each demand $d \in \mathcal{D}$ is split into a number of non-zero path-flows $f(d, p, 0)$, $p \in \mathcal{P}'(d, 0)$, where $\mathcal{P}'(d, 0)$ is the set of paths between the end-nodes of demand d, and that the resulting link-flows do not exceed link capacities. This conditions are expressed like this:

$$\sum_{p \in \mathcal{P}'(d,0)} f(d, p, 0) = h(d), \quad d \in \mathcal{D} \tag{16a}$$

$$\sum_{d \in \mathcal{D}} \sum_{p \in \mathcal{R}'(e,d,0)} f(d, p, 0) \leq c(e), \quad e \in \mathcal{E}. \tag{16b}$$

Note that in the second condition, $\mathcal{R}'(e, d, 0)$ is the set of those paths in $\mathcal{P}'(d, 0)$ that pass through link e, hence the left-hand side of (16b) expresses the load of link e.

In fact, in the network setup so described, the total number of necessary (non-zero) path-flows $f(d, p, 0)$ is no more than $D + E$ (see [50]), so the path lists $\mathcal{P}'(d, 0)$ are very limited as most of them only contain one path. Hence, since our goal is to protect traffic in the states of limited link availability, we need to find path lists appropriate to each state $s \in \mathcal{S}$. This is necessary for obvious reasons, such as because a single path used for a given demand in the normal state may not be available in some other states. We use the following linear programming (LP) formulation to define the path lists.

PATH LISTS GENERATION

$$\min \sum_{e \in \mathcal{E}} \xi(e) y_e^0 \tag{17a}$$

$$[\lambda_d^0] \sum_{p \in \mathcal{P}(d,0)} x_{dp}^0 \geq h(d), \quad d \in \mathcal{D} \tag{17b}$$

$$[\pi_e^0] \sum_{d \in \mathcal{D}} \sum_{p \in \mathcal{R}(e,d,0)} x_{dp}^0 \leq y_e^0, \quad e \in \mathcal{E} \tag{17c}$$

$$[\lambda_d^s] \sum_{p \in \mathcal{P}(d,s)} x_{dp}^s \geq h(d), \quad d \in \mathcal{D}(s), s \in \mathcal{S} \tag{17d}$$

$$[\pi_e^s] \sum_{d \in \mathcal{D}(s)} \sum_{p \in \mathcal{R}(e,d,s)} x_{dp}^s \leq \alpha(e, s) y_e^0,$$
$$e \in \mathcal{E}(s), s \in \mathcal{S} \tag{17e}$$

$$y^0 \geq 0; \; x^0 \geq 0; \; x^s \geq 0, s \in \mathcal{S}. \tag{17f}$$

Above, variables in vector $y^0 = (y_e^0, \; e \in \mathcal{E})$ represent link capacities, while variables in vectors $x^0 = (x_{dp}^0, \; d \in \mathcal{D})$ and $x^s = (x_{dp}^s, \; d \in \mathcal{D}(s), s \in \mathcal{S})$ represent path-flows that realize traffic demands in the normal state and in the degradation states, respectively, which is ensured by constraints (17b) and (17d). Constraints (17c) and (17e), make sure that link loads (expressed by the left-hand sides of the considered constraints) do not exceed the capacity available on the links. Note that the variables that make up the vector x^0 correspond to path-flows $f(d, p, 0)$ in an operating network, and hence constraints (17b) and (17c) correspond to conditions (16a) and (16b).

The (non-compact) linear program formulated in this way is solved by column generation. For that, the quantities appearing in square brackets in front of the constraints, which denote the dual variables associated with them, are used. Initially, each list $\mathcal{P}(d, 0)$ and $\mathcal{P}(d, s)$, $s \in \mathcal{S}$, contains only one path, which is a shortest (in terms of link weights equal to the unit link costs ξ) path between the end nodes of the

considered demand. Note that for a given $s \in \mathcal{S}$, such a path can only use links in $\mathcal{E}(s)$. Then the LP formulation (17) is iteratively solved, extending the path lists in each iteration. After solving (17), the optimal values of the dual variables π_e^0 are used as the weights in finding a shortest path for each demand $d \in \mathcal{D}$. Similarly, for each $s \in \mathcal{S}$, the optimal values of the dual variables π_e^s are used as the weights in finding a shortest path for each demand $d \in \mathcal{D}(s)$. If the length of a path thus found is strictly less than the optimal value of the corresponding dual variable λ_d^0 or λ_d^s, then the path is added to the appropriate path list. After that, the algorithm is iterated, until no such path is found. (Details about the described algorithm can be found in Chapter 10.1 of [50].) Note also that among the paths on the lists $\mathcal{P}(d, s)$ there are no paths containing links with $\alpha(e, s) = 0$.

In all the optimization formulations considered below, we will use the following extension of the path lists thus obtained:

- Step 1: $\mathcal{P}(d, 0) := \mathcal{P}(d, 0) \cup \bigcup_{s \in \mathcal{S}} P(d, s), \; d \in \mathcal{D}$.
- Step 2: $\mathcal{P}(d, s) := \mathcal{P}(d, s) \cup (\mathcal{P}(d, 0) \setminus \{p \in \mathcal{P}(d, 0) : \mathcal{E}(d, p) \cap (\mathcal{E} \setminus \mathcal{E}(s)) \neq \varnothing\}), \; d \in \mathcal{D}(s)$.

Note that in Step 1 we assume $\mathcal{P}(d, s) = \varnothing$ for $d \notin \mathcal{D}(s)$. This extension ensures that, on one hand, path lists for the normal state include all paths generated by (17) for all states in $\mathcal{S}$, and, on the other hand, for any state in $\mathcal{S}$ all its path lists include all paths used in the normal state besides the paths that contain at least one link with capacity degraded to 0.

The problem formulated in (17) finds a cheapest link capacity vector y^0 that ensures realization of the traffic demand vector $h = (h(d), \; d \in \mathcal{D})$ in the normal state and in all states from the assumed list $\mathcal{S}$. The way the traffic demands are realized is specified by the optimized path-flows vectors x^0 and x^s, $s \in \mathcal{S}$. Note that the traffic routing and protection mechanism adopted in (17) allows for restoring the path-flows in each state s from scratch, because the flow patterns x^0, x^s, $s \in \mathcal{S}$, are independent of each other. While this mechanism, known as Global Rerouting or Unrestricted (Flow) Reconfiguration [50], is most effective in restoring traffic, it is practically not applicable to real networks. Therefore, we do not consider this mechanism for traffic protection, but use formulation (17) only to create path lists that will be used for the (practical) traffic routing and protection mechanism we choose.

The chosen mechanism, known as affine flow thinning (AFT) [57], in the form assumed in this paper relates the path-flow on a given path $p \in \mathcal{P}(d, s)$, $d \in \mathcal{D}(s)$, $s \in \mathcal{S}$, to its normal flow $f(d, p, 0)$ through the following affine formula [64]:

$$f(d, p, s) = f(d, p, 0) - \sum_{e \in \mathcal{E}(d,p)} z(d, p, e)\beta(e, s),$$
$$p \in \mathcal{P}(d, s), \quad d \in \mathcal{D}(s), \; s \in \mathcal{S}. \tag{18}$$

The formula defines, for a given path $p \in \mathcal{P}(d, 0)$, its flow $f(d, p, s)$ in a given state $s \in \mathcal{S}$. (By definition, this flow is equal to 0 when $d \notin \mathcal{D}(s)$.) This flow is an affine function of link degradation coefficients $\beta(e, s), e \in \mathcal{E}(d, p)$ (where

$\beta(e, s) = 1 - \alpha(e, s)$, and $\mathcal{E}(d, p)$ is the set of links composing the considered path) with the coefficients $f(d, p, 0)$ (normal flow on the considered path) and $z(d, p, e) \geq 0$, $e \in \mathcal{E}(d, p)$. Note that by definition $f(d, p, s) \leq f(d, p, 0)$ which means that the path-flow in the degraded states is not greater than the normal path-flow (i.e., the flow is thinned). Moreover, each thinned path-flow depends only on the (state-dependent) degradation coefficients of the links composing the path on which the flow is realized.

Coefficients $z(d, p, e)$, $p \in \mathcal{P}(d, s)$, $d \in \mathcal{D}(s)$, $e \in \mathcal{E}(d, p)$, together with the path-flows $f(d, p, 0)$, $p \in \mathcal{P}(d, 0)$, $d \in \mathcal{D}$, used in the normal state, determine the path-flows for all states in $\mathcal{S}$, provided that $\mathcal{P}(d, s) \subseteq P(d, 0)$. Recall that the last condition is met thanks to the above-described extension of the path lists generated by solving formulation (17).

Now let us consider the final step in the preprocessing process, which is to re-optimize (adjust) the capacity installed on the links in the existing network (specified by the vector $c = (c(e), e \in \mathcal{E}$, where $c(e)$ is the number of modules installed on link e) in order to prepare room for improving traffic throughput in the degradation states. This adjustment is done within a given budget equal to $B + \Delta$, where $B = \sum_{e \in \mathcal{E}} \xi(e)c(e)$ is the cost of the existing link capacity and Δ is an assumed percentage of B allowing for capacity expansion, by solving the following MIP formulation.

LINK CAPACITY ADJUSTMENT

$$\max \ t \qquad (19a)$$

$$\sum_{e \in \mathcal{E}} \xi(e)y_e^0 \leq B + \Delta \qquad (19b)$$

$$\sum_{p \in \mathcal{P}(d,0)} x_{dp}^0 \geq h(d), \quad d \in \mathcal{D} \qquad (19c)$$

$$\sum_{d \in \mathcal{D}} \sum_{p \in \mathcal{R}(e,d,0)} x_{dp}^0 \leq y_e^0, \quad e \in \mathcal{E} \qquad (19d)$$

$$\sum_{p \in \mathcal{P}(d,s)} x_{dp}^s \geq h(d, s)t, \quad d \in \mathcal{D}(s), \ s \in \mathcal{S} \qquad (19e)$$

$$\sum_{d \in \mathcal{D}(s)} \sum_{p \in \mathcal{R}(e,d,s)} x_{dp}^s \leq \alpha(e, s)y_e^0$$
$$e \in \mathcal{E}(s), s \in \mathcal{S} \qquad (19f)$$

$$x_{dp}^s = x_{dp}^0 - \sum_{e \in \mathcal{E}(d,p)} \beta(e, s)z_{dp}^e,$$
$$d \in \mathcal{D}(s), \quad p \in \mathcal{P}(d, s), \ s \in \mathcal{S} \qquad (19g)$$

$$t \geq 0; \quad y^0 \geq 0 \text{ and integer}; \ x^0 \geq 0;$$
$$x^s \geq 0, \quad s \in \mathcal{S}; z \geq 0. \qquad (19h)$$

Above, the vector $y^0 = (y_e^0, e \in \mathcal{E})$ expresses the number of modules installed on the links after the adjustment. The total cost of such optimized capacity is limited by inequality (19b). Furthermore, the meaning of the path-flow variables that make up the vectors $x^0 = (x_{dp}^0, d \in \mathcal{D})$ and $x^s = (x_{dp}^s, d \in \mathcal{D}(s), s \in \mathcal{S})$ is the same as in formulation (17). With this interpretation and the so defined link capacity, constraints (19c), (19d) and (19f) have the same meaning as in formulation (17).

However, now constraint (19e) and its counterpart (17d) are different. Since in general, because of the limited budget B, it will not be possible to assure traffic throughput specified

by h when link availability is reduced, we allow for reducing the traffic throughput by factor t, which is a variable that is maximized in objective (19a). In fact, this reduction depends also on a state-dependent constant factor $T(s)$ as follows:

$$T(s) = w(s)F(s), \quad s \in \mathcal{S} \qquad (20a)$$

$$F(s) = \frac{\sum_{e \in \mathcal{E}} \alpha(e, s)c(e)}{\sum_{e \in \mathcal{E}} c(e)}, \quad s \in \mathcal{S} \qquad (20b)$$

$$h(d, s) = T(s)h(d), \quad d \in \mathcal{D}(s), \quad s \in \mathcal{S}. \qquad (20c)$$

In (20a), the parameters $w(s)$ are proportional to the occurrence frequency of state s during the considered period of time of network operation, while the quantity $F(s)$ (defined in (20b)) is the proportion of the total installed capacity available in state s with respect to the total capacity installed. In effect, for the maximum value t^* of the maximized variable t, the fraction $T(s)t^*$ of the traffic demand $h(d)$ is restored in state s.

Finally, constraint (19g) assures that the path-flows are thinned according to the AFT rule (18). Note that the AFT formulae are optimized by means of variables $z = (z_{dp}^e, d \in \mathcal{D}(s), s \in \mathcal{S}, e \in \mathcal{E})$, which correspond to the constant affine coefficients $z(d, p, e)$ in definition (18).

C. MAX-MIN FAIR OPTIMIZATION OF TRAFFIC PROTECTION

After the preprocessing phase described in Section IV-B, we are now able to tackle the main issue of the proposed optimization approach, that is max-min fair traffic throughput optimization for the states with limited link capacity included in the list $\mathcal{S}$.

Thus, as the result of preprocessing, we consider the network with adjusted link capacities $C(e) = y^{0*}, e \in \mathcal{E}$, where the vector y^0 is optimized through formulation (19), and the same path lists as in (19). Moreover, we modify the values of $F(s)$ in coefficients $T(s)$ for link capacities adjusted in this way:

$$F(s) = \frac{\sum_{e \in \mathcal{E}} \alpha(e, s)C(e)}{\sum_{e \in \mathcal{E}} C(e)}, \quad s \in \mathcal{S}. \qquad (21)$$

Let $\mathcal{Q} = \{(d, s) : d \in \mathcal{D}(s), s \in \mathcal{S}\}$ be the set of all demand-state pairs for which traffic protection is to be provided, and let $t = (t(d, s), (d, s) \in \mathcal{Q})$ be the vector of coefficients specifying the fractions of the traffic volume $h(d, s)$ (defined in (20c)) realized for demand-state pairs (d, s). We will call such a vector feasible if the following system of linear equations/inequalities is feasible:

$$\text{constraints} \ (19c), (19g) \qquad (22a)$$

$$\sum_{d \in \mathcal{D}} \sum_{p \in \mathcal{R}(e,d,0)} x_{dp}^0 \leq C(e), \quad e \in \mathcal{E} \qquad (22b)$$

$$\sum_{p \in \mathcal{P}(d,s)} x_{dp}^s \geq h(d, s)t(d, s), \quad (d, s) \in \mathcal{Q} \qquad (22c)$$

$$\sum_{d \in \mathcal{D}(s)} \sum_{p \in \mathcal{R}(e,d,s)} x_{dp}^s \leq \alpha(e, s)C(e),$$
$$e \in \mathcal{E}(s), \quad s \in \mathcal{S} \qquad (22d)$$

Clearly, the feasibility of t means that the traffic demand vector h and the reduced traffic demand vectors

$h(s) = (h(d,s)t(d,s)), s \in \mathcal{S})$ can be realized in the normal and the degraded states, respectively, by means of some feasible AFT path-flows $x^0, x^s, s \in \mathcal{S}$.

A question arises as to what property of feasible vectors should be used to choose the most appropriate one from a traffic protection viewpoint. Our (natural) answer is *max-min fairness* (MMF) [50]. In order to explain what MMF actually means in the considered optimization model, let us consider the set $\mathcal{F}$ of feasible vectors t, i.e., a polyhedron in the Euclidean space of dimension $N = \sum_{s \in \mathcal{S}} |\mathcal{D}(s)|$ (i.e., $\mathbb{R}^N$) obtained by projecting the polyhedron defined by the system (22) onto $\mathbb{R}^N$. Moreover, let $\vec{t}$ denote the vector obtained from t by arranging its elements in nondecreasing order. Then vector $t^* \in \mathcal{F}$ is called *lexicographically maximal (lex-max)* if, and only if, $\vec{t}^* \succeq \vec{t}$ for all $t \in \mathcal{F}$, where '$\succeq$' denotes the lexicographical order. It can be shown that (thanks to the convexity of polyhedron $\mathcal{F}$), a lex-max vector is also a max-min fair vector in $\mathcal{F}$ (see [54], [56] for details). For finding a lex-max vector, we will use an algorithm (called the MMF algorithm) based on iterative solving of the following LP formulation, where the sets $\mathcal{Q}'$ and $\mathcal{Q}''$ constitute a partition of the set $\mathcal{Q}$.

Basic MMF problem: MMFP($\mathcal{Q}', \mathcal{Q}''$)

$$\max \quad t \tag{23a}$$

$$\sum_{p \in \mathcal{P}(d,0)} x_{dp}^0 \geq h(d), \quad d \in \mathcal{D} \tag{23b}$$

$$\sum_{d \in \mathcal{D}} \sum_{p \in \mathcal{R}(e,d,0)} x_{dp}^0 \leq C(e), \quad e \in \mathcal{E} \tag{23c}$$

$$\sum_{p \in \mathcal{P}(d,s)} x_{dp}^s \geq h(d,s)t, \quad (d,s) \in \mathcal{Q}' \tag{23d}$$

$$\sum_{p \in \mathcal{P}(d,s)} x_{dp}^s \geq h(d,s)t^*(d,s), \quad (d,s) \in \mathcal{Q}'' \tag{23e}$$

$$\sum_{d \in \mathcal{D}(s)} \sum_{p \in \mathcal{R}(e,d,s)} x_{dp}^s \leq \alpha(e,s)C(e),$$
$$e \in \mathcal{E}(s), \quad s \in \mathcal{S} \tag{23f}$$

$$x_{dp}^s = x_{dp}^0 - \sum_{e \in \mathcal{E}(d,p)} \beta(e,s)z_{dp}^e,$$
$$d \in \mathcal{D}(s), \quad p \in \mathcal{P}(d,s), \quad s \in \mathcal{S} \tag{23g}$$

$$t \geq 0; \ x^0 \geq 0; \quad x^s \geq 0, \ s \in \mathcal{S}; \ z \geq 0. \tag{23h}$$

The above formulation is similar to formulation (19), with one important difference: the traffic volumes realized for the demand-state pairs in the set $\mathcal{Q}'$ are lifted by maximizing the value of variable t (constraint (23d)), while for the remaining pairs the realized traffic volume is just lower bounded by the fixed parameter $t^*(d,s)$ (constraint (23e)).

The following MMF algorithm will find a lex-max vector t^* for the considered traffic protection problem. (In the algorithm, $\lambda_d^s, (d,s) \in \mathcal{Q}'$, denote the dual variables corresponding to the constraints in (23e).)

The explanation of MMFA is as follows (see [50]). During the first passage of the algorithm, in Step 1, formulation MMFP($\mathcal{Q}, \varnothing$) is solved, whose optimal solution t^* lifts the traffic volumes $h(d,s)$ at an equal pace for all demand-state pairs in $\mathcal{Q}$. Then the pairs for which the $h(d,s)$ (i.e., $t^*(d,s)$ cannot be lifted any further) are identified: these are the pairs for which λ_d^{s*} is strictly greater than 0 (this follows

---

MMF Algorithm (MMFA)

Step 0: Initialization: $\mathcal{Q}' := \mathcal{Q}$ and $\mathcal{Q}'' := \varnothing$.
Step 1: Solve MMFP($\mathcal{Q}', \mathcal{Q}''$); let t^* denote the optimal value of objective (23a) and λ_d^{s*} the optimal value of the dual variable λ_d^s.
Step 2: Let $\widehat{\mathcal{Q}} := \{(d,s) \in \mathcal{Q}' : \lambda_d^{s*} > 0\}$, and put $t^*(d,s) := t^*, (d,s) \in \widehat{\mathcal{Q}}; \mathcal{Q}' := \mathcal{Q}' \setminus \widehat{\mathcal{Q}}, \mathcal{Q}'' := \mathcal{Q}'' \cup \widehat{\mathcal{Q}}$.
Step 3: If $\mathcal{Q}' \neq \varnothing$ go to Step 1. Otherwise stop: $t^* := (t^*(d,s), (d,s) \in \mathcal{Q})$ is the MMF solution we are looking for.

---

from the complementary slackness property). Then, in Step 2, the pairs identified in this way are moved from the set $\mathcal{Q}'$ (equal to $\mathcal{Q}$ in the first passage) to the set $\mathcal{Q}''$ (which is empty in the first passage) and the value t^* is assigned to the corresponding elements in the constructed lex-min vector t^*. Finally, in Step 3, it is checked whether or not the vector t^* has been fully specified, and if not, the next iteration is started in Step 1.

It should be clarified here that $\lambda_d^{s*} = 0$ does not necessarily mean that the current maximum t^* for this particular demand-state pair can be improved in the future iterations. Yet, in the next iteration, in the set $\mathcal{Q}' \setminus \widehat{\mathcal{Q}}$ there will appear at least one demand-state pair (d', s') (possibly (d,s)) with $\lambda_{d'}^{s'*} > 0$. This is due to the dual constraint $\sum_{(d,s) \in \mathcal{Q}'} \lambda_d^s = 1$ and the nonnegativity of the considered dual variables. In fact, this observation also means that MMFA will eventually stop.

Let us finally note that MMFA is an instance of a general MMF algorithm for convex problems described in detail in [54], [56].

D. DISCUSSION

Let us briefly return to three issues: the choice of AFT as a traffic routing/protection mechanism, the choice of MMF for measuring traffic protection performance, and the computational complexity of our optimization model.

The reasons for choosing the AFT mechanism are as follows (see [57], [64]):

- The considered AFT mechanism controls the individual path-flows $f(d,p,0), d \in \mathcal{D}, p \in \mathcal{P}(d,0)$, at their source nodes.
- The information required at the source node to adjust a given flow $f(d,p,0)$ according to formula (18) in any state $s \in \mathcal{S}$ consists merely of the degradation coefficients $\beta(e,s)$ of the links included in the path $p \in \mathcal{P}(d,0)$.
- This information can be sent back to the path's originating node from the path's transit nodes as soon as the degradation coefficient of any of the path's links has changed (up or down).
- Because such backwards signalling can be made virtually instantaneous, the current path-flows are adjusted on-line.

- When one of the path's links becomes totally unavailable, then the path's originating node is immediately informed about this by the originating node of the unavailable link closest to the path's originating node and the flow is cancelled.
- Because the flows on the degraded paths are in general thinner than the normal flows, formula (18) can be (relatively) safely used in the degradation states that are not taken into account in the optimization process.

In summary, once the affine coefficients z are optimized by means of MMFA, the resulting AFT formulae can be used at the path's originating nodes for on-line flow adjustments in any link degradation state. This property is hardly achievable by any other mechanism.

The advantages of MMF, in turn, can be summarized like this (see [54], [56]):

- The MMF vector t^* found by MMFA has the following property (see [56]): any of its elements $t^*(d, s)$ cannot be increased without decreasing some element $t^*(d', s')$ that is less than $t^*(d, s)$.
- Having this in mind, and taking the definition (21) of the $T(s)$ coefficients that express the importance of a given state $s \in \mathcal{S}$ (i.e., $w(s)$), as well as its fraction of available capacity (i.e., $F(s)$), the MMF vector t^* maximizes the traffic throughput $h(d, s)t^*(d, s)$ realized for each demand-state pair (d, s) in a fair way.

In fact, instead of the pure max-min fairness measure applied in MMFA, its variant, called *max-total fairness* (MTF) here, could be considered. The difference is that in MTF, vector $t' = (\sum_{d \in \mathcal{D}(s)} h(d, s), s \in \mathcal{S})$ is the subject of MMFA, and not vector $t = (t(d, s), d \in \mathcal{D}(s), s \in \mathcal{S})$. In effect, an optimal vector t' will lexicographically maximize the total volumes of traffic realized in the individual states, and not the traffic volumes of individual demands in individual states. Although this variant is computationally much faster than MMF (as now MMFA requires at most S iterations), its use can result in allowing no traffic at all for some demands in some states to be realized.

Finally, let us consider the computational complexity of the presented optimization model. The main observation here is that among the three main optimization problems, i.e., path list generation (17), link capacity adjustment (19) and basic MMF problem (23), the second one is $\mathcal{NP}$-hard (see Section 4.3.1 in [50]) while the remaining two are polynomial (as compact linear programming problems). Nevertheless, as illustrated at the end of Section V-D, in practice solving (19) is rather fast and most of the time of the whole numerical procedure is spent in MMFA because of a large number of iterations required to achieve an optimal MMF vector t^*.

V. NUMERICAL STUDY
In this section, we will illustrate an application of the proposed approach for traffic protection, using an FSO network instance created on the basis of realistic network

topology, traffic data, and weather state description. All the reported calculations were executed on a PC-class computer (Windows 10 64-bit, 16 GB RAM, Processor Intel Core i7-10510U, four 2.3GHz logical processors) using CPLEX 12.6.3.0.

A. DESCRIPTION OF THE NETWORK INSTANCE
The considered network instance, depicted in Fig. 5, was first presented in [45]. It consists of $V = 12$ nodes selected from the Paris Metropolitan Area (PMA), interconnected by $E = 21$ undirected links representing sets of parallel bi-directed (full-duplex) FSO links (in the figure, the number inside a link specifies its index). The symmetric traffic matrix (specified in Table 4) of the PMA network (PMAN) was prepared taking into account realistic demographic data (see [45]).
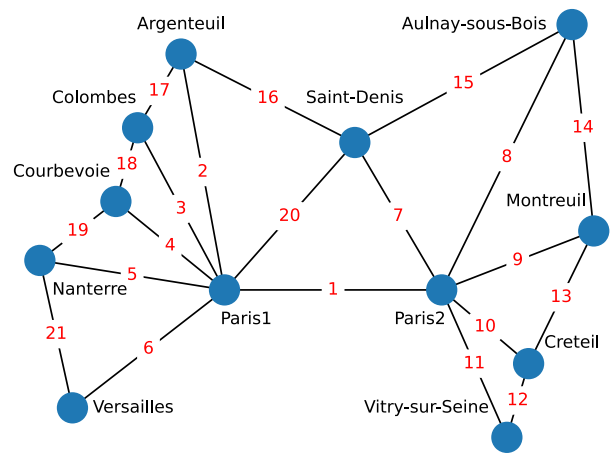
FIGURE 5. Paris metropolitan area network.

TABLE 4. PMAN traffic matrix [Gbps].

	(1)	(2)	(3)	(4)	(5)	(6)	(7)	(8)	(9)	(10)	(11)	(12)
(1) Paris1	–	10	9	9	7	7	8	7	8	8	9	7
(2) Paris2	10	–	9	9	7	7	8	7	8	8	9	7
(3) Saint-Denis	9	9	–	8	6	6	7	6	7	7	8	6
(4) Argenteuil	9	9	8	–	6	6	7	6	7	7	8	6
(5) Colombes	7	7	6	6	–	4	5	4	5	5	6	4
(6) Courbevoie	7	7	6	6	4	–	5	4	5	5	6	4
(7) Nanterre	8	8	7	7	5	5	–	5	6	6	7	5
(8) Versailles	7	7	6	6	4	4	5	–	5	5	6	4
(9) Vitry-Sur-Seine	8	8	7	7	5	5	6	5	–	6	7	5
(10) Creteil	8	8	7	7	5	5	6	5	6	–	7	5
(11) Montreuil	9	9	8	8	6	6	7	6	7	7	–	6
(12) Aulnay-Sous-Bois	7	7	6	6	4	4	5	4	5	5	6	–

The link availability state list $\mathcal{S}$ used in the numerical experiments was prepared (using the hourly weather data records for PMA available in the database accessible at *www.worldweatheronline.com*) in the following way:

1) We consider the weather conditions observed during a one year period, from January 1, 2016 until December 31, 2016, where among all 8784 hourly weather states, 804 states are identified as *adverse*

(weather) states; the remaining 7980 are the normal states, i.e., with no fog, rain or snow reported.

2) For each ('foggy', 'rainy' or 'snowy') state s, its link availability coefficients $\alpha(e, s)$, $e \in \mathcal{E}$, are calculated (using the data in the corresponding weather records) by means of our general methodology described in Section III. The so obtained coefficients are rounded to two meaningful digits and all $\alpha(e, s)$ less than the assumed transmission quality threshold 0.25 are set to 0.

3) Out of 804 adverse states, 187 states turn out to be *connected* (i.e., the network graph remains connected after deleting all links with $\alpha(e, s) = 0$), while the remaining 617 states become *disconnected* (which means that in these states the network graph is split into two or more disjoint connected components). Moreover, out of 617 disconnected states, 68 states are fully disconnected ($\alpha(e, s) = 0$ for all $e \in \mathcal{E}$). Hence, since it is not possible to realize any traffic in such states, we delete them and in effect consider only $617 - 68 = 549$ disconnected states.

4) In effect, $S = 206$ representative link availability states are identified and included in the final list of states $\mathcal{S}$. By definition, each such state s represents the subset of $N(s)$ adverse states with the same link availability vector $\boldsymbol{\alpha}(s)$, and hence the vectors $\boldsymbol{\alpha}(s)$ for all states s in $\mathcal{S}$ are mutually different. More precisely, in the so-defined list $\mathcal{S}$, there are $S' = 101$ states representing the 187 connected foggy states, and $S'' = 105$ states representing the 549 disconnected foggy states. Note that $\sum_{s \in \mathcal{S}} N(s) = 736$.

5) Next, we delete from $\mathcal{S}$ all states with $N(s) = 1$ (i.e., the states that appear only once a year).

6) In effect, $S = 75$ states remain on the constructed list and they represent 605 hourly weather states. Out of them, $S' = 30$ states are connected (they represent 116 hourly states), and $S'' = 45$ states are disconnected (they represent 489 hourly states). Note that now $\sum_{s \in \mathcal{S}} N(s) = N = 605$.

7) Finally, the resulting values of the $w(s)$ parameters are as follows: $w(s) = \frac{N(s)}{N}$, $s \in \mathcal{S}$.

In the calculations of link availability coefficients performed in the second step of the above procedure for state list preparation, we used a simple ad-hoc approach for estimating the visibility function $V(z)$ (and, for that matter, also for estimating the precipitation rates $\varphi(z)$, $\psi(z)$), which is as follows.

We consider the actual locations of all 168 M-points in PMA depicted in Fig. 6 (the locations of the M-points are the same as in Fig. 3), together with the actual positions of the PMAN nodes and links. Note that the nodes are numbered in the same way as in Table 4 but now they are placed in their actual geographical locations; this is why the PMAN configuration in Fig. 6 looks different than the schematic (but nicer) configuration depicted in Fig. 5.
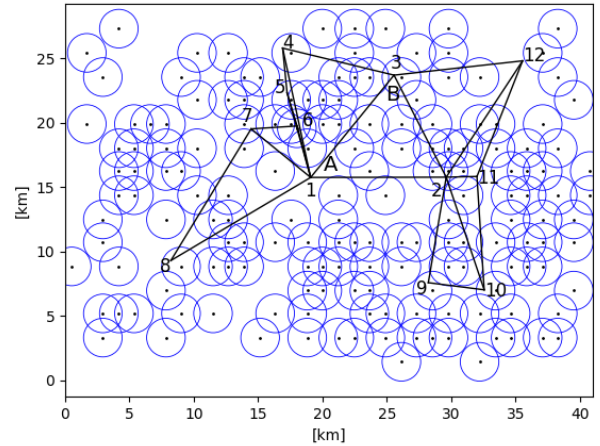
FIGURE 6. PMAN: M-points, nodes, links.
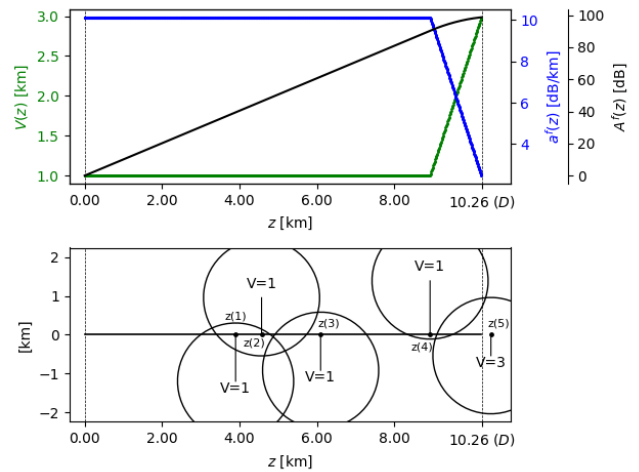
FIGURE 7. Analysis of link AB: actual visibility at the M-points in the center of the intersected circles, November 2, 2016, 4:00 am.

Next, we find the minimum value of radius R, for which each of the 21 PMAN links intersects at least 3 circles of radius R with the center in one of the M-points. This value turns out to be equal to 1.5 km and the resulting circles are illustrated in Fig. 6. For the obtained configuration of circles, for each link we identify the circles it intersects. Then, to estimate the values of the parameter of interest (one of V, φ or ψ) at all points along a given link, we use the values of this parameter measured only in the M-points placed in the centers of the intersected circles. We note here that the idea of using such circles for whether state characterization can be found in Section 3.2 of paper [77], where the radius of 500 m was considered for measurement points located in urban areas. In our calculations, we allow for increasing this value in order to get a reasonable number of measurements (at least 3) for every link.

Let us illustrate the idea how this is done in the two following examples that analyze visibility along the link between node A (Paris1) and B (Saint-Denis) of length $D = 10.26$ km marked in Fig. 6 (and, for that matter, also in Fig. 3). Its translated/rotated version (obtained in the way explained in

Section III-C) is shown in the lower part of Fig. 7, together with the five circles it intersects (these circles are visible in Fig. 6). In order to plot the visibility function $V(z)$ analogous to that depicted (for the same link) in the upper part of Fig. 4, we first project the centers of the considered circles onto the z-axis; these projections are placed on the z-axis at the following distances (expressed in [km]) from the origin: $z(1) = 3.90$, $z(2) = 4.57$, $z(3) = 6.10$, $z(4) = 8.92$, $z(5) = 10.50$. Next, we assign the visibility value observed at the centre of each circle (shown in the figure) to its projection point. In effect, we get $V(z(1)) = V(z(2)) = V(z(3)) = V(z(4)) = 1, V(z(5)) = 3$. Then, we notice that there are two projection points, $z(1)$ and $z(2)$, that lie inside a segment of the link that belongs to two circles (with the centers on the opposite sides of the link). In general, to be on the safe side, in this case we would delete the projection point with larger visibility from further consideration, but since in our particular case both projections are assigned the same visibility, we leave both projections for further use. (In fact, if the two circles had their centers on the same side of the link, we would delete the projection point whose distance to the center of its circle is larger, and leave both projections when their visibilities are equal.) After that, we set the visibility of the end nodes of the link, $V(0)$ to $V(z(2))$ and $V(D)$ to $V(z(5))$, i.e., to the visibilities assigned to the nearest projection points.

Finally, we define visibility function $V(z)$ as the piece-wise linear function with breakpoints at $z(2)$, $z(3)$, $z(4)$. This function is plotted in the upper part of Fig. 7, together with functions $a^f(z)$ and $A^f(z)$ defined in Section III-C by formulas (10) and (12), respectively. As the result we get the value $A^f(D) = 98.7$ dB, for which the link availability coefficient $\alpha(A^f(D))$ is calculated by means of the formulas presented in Section III-B. The consecutive calculation steps, based on formulas (5)-(9), are as follows:

1) $SNR_n = 45 - 2 \times 98.7 = -152.4$ [dB]
2) $SNR'_n = 10^{\frac{SNR_n}{10}} = 5.754 \cdot 10^{-16}$
3) $BER = \frac{1}{2} \operatorname{erfc}\left(\sqrt{\frac{SNR'_n}{8}}\right) = \frac{1}{2} \operatorname{erfc}\left(\sqrt{0.72 \cdot 10^{-16}}\right) \approx 0.5$
4) $\alpha(98.7) = (1 - BER)^{512} = \left(\frac{1}{2}\right)^{512} \approx 0$.

The visibility values at the five considered M-points (i.e., 1, 1, 1, 1, 3) in Fig. 7 are the real values specified in the weather records for November 2, 2016, 4:00 am. In the second example, considered in Fig. 8, we alter these values to 3.6, 4.2, 5.0, 4.7, 5.715 in order to obtain another, more complicated, visibility function $V(z)$ and the corresponding functions $a^f(z)$ and $A^f(z)$; these functions are shown in the upper part of Fig. 8. In this case $A^f(D) = 14.72$ dB and

1) $SNR_n = 45 - 2 \times 14.72 = 15.56$ [dB]
2) $SNR'_n = 10^{\frac{SNR_n}{10}} = 35.97$
3) $BER = \frac{1}{2} \operatorname{erfc}\left(\sqrt{\frac{SNR'_n}{8}}\right) = \frac{1}{2} \operatorname{erfc}\left(\sqrt{4.5}\right) = 1.355 \cdot 10^{-3}$
4) $\alpha(14.72) = (1 - BER)^{512} = 0.99865^{512} = 0.5$.
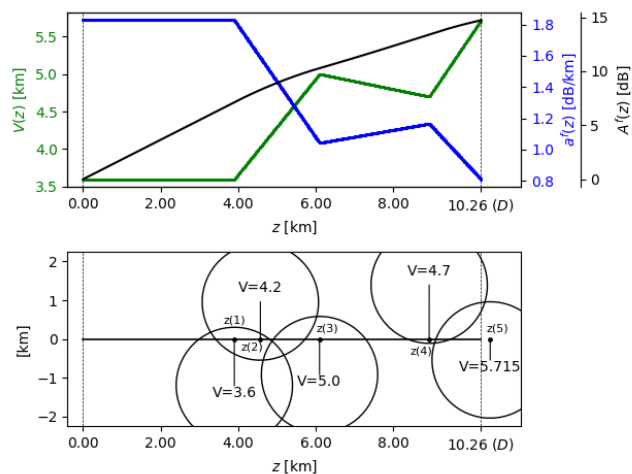

FIGURE 8. Analysis of link AB: modified visibility at the M-points in the center of the intersected circles.

Observe that the value $A^f(D) = 14.72$ dB lies in the critical region of the arguments of the BER function shown in Fig. 1 in Section III.A, i.e., in the region where the BER value is very sensitive to attenuation.

In the considered PMA network, the demands are directed since they model Internet traffic. Moreover, the links are bi-directed (i.e., each link represents two oppositely directed arcs of the same capacity) since they are composed of parallel full-duplex FSO transmission systems (i.e., each such system realizes two oppositely directed transmissions of the same data rate). On the other hand, the optimization problem formulations in Section IV assume undirected links (note that then the direction of demands is not important). This, however, is not an issue. As explained in [78], the network with bi-directed links and directed but symmetric traffic matrix can be transformed to an equivalent network with undirected links and undirected demands. In such a network, each original bi-directed link (of capacity $c(e)$ in each direction) is replaced by an undirected link of capacity $c(e)$, and the original directed symmetric traffic matrix is reduced to its upper part, whose elements represent undirected traffic demands. Then, any optimal solution of any of the optimization formulations in Section IV applied to the transformed network is optimal for the considered network configuration. To obtain such a directed solution, the demands from the upper part of the traffic matrix are made directed again and the path-flows x^0, x^s, $s \in \mathcal{S}$, are made directed accordingly. Then, the reversed copies of the so defined path-flows are used to realize the directed demands from the lower part of the traffic matrix. Finally, the resulting directed link-flows are assigned to the appropriate arcs of the bi-directed links in the original network.

In the numerical experiments discussed below, we assume that the capacity (in each direction) of one full-duplex FSO system is 10 Gbps, and its cost is the same for all links and equal to 1 (i.e., $\xi(e) = 1$, $e \in \mathcal{E}$). Moreover, to be consistent
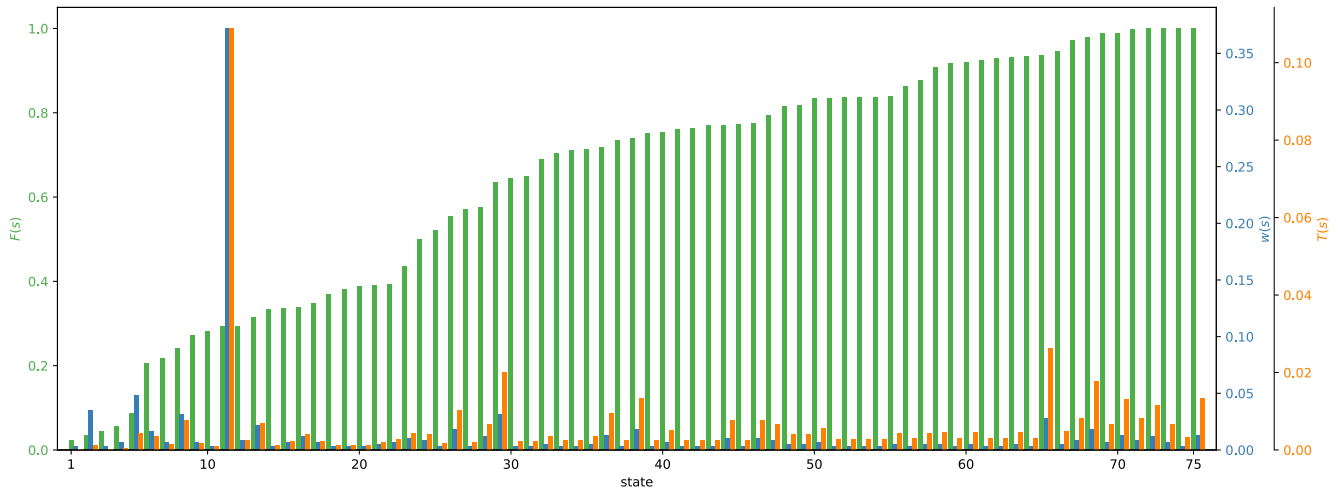
FIGURE 9. $F(s)$, $w(s)$ and $T(s)$ for all $s \in \mathcal{S}$; $\Delta = 10\%$.

with the formulations of Section IV, for the purpose of optimization we will re-scale the elements of the traffic matrix by dividing them by 10. In this way, the unit of the demand volume becomes equal to 10 Gbps, and the modularity of links becomes equal to one such unit. In other words, now $c(e)$ (or $C(e)$) means that each link e is composed of $c(e)$ (or $C(e)$) parallel FSO transmission systems and its capacity is actually equal to $10 \times c(e)$ (or $10 \times C(e)$) Gbps.

Below, the (undirected) demands will be numbered according to the lexicographical order of the elements in the upper part of the traffic matrix, i.e., each index d (where $1 \leq d \leq D$ and $D = 66$) denotes, respectively, the node-pairs $\{1, 2\}, \{1, 3\}, \ldots, \{1, 12\}, \{2, 3\}, \{2, 4\}, \ldots, \{11, 12\}$. Thus, the demand vector $\boldsymbol{h} = (h(d), d = 1, 2, \ldots, 66)$ (specified by the upper triangle of Table 4) is equal to $(10, 9, \ldots, 7, 9, 9, \ldots, 6)$. Note that the total traffic volume is equal to 42.9 units, i.e., to 429 Gbps.

B. PATHS AND LINK CAPACITIES PREPROCESSING
In the preprocessing phase of our approach, we first construct the path lists $\mathcal{P}(d, 0)$, $\mathcal{P}(d, s)$, $d \in \mathcal{D}(s)$, $s \in \mathcal{S}$. This is done by means of formulation (17) solved by path generation, and after that appropriately extended, by the two-step procedure described in Section IV-B, for the normal state and all states in $\mathcal{S}$. The so obtained path lists consist of 1 to 11 paths each (310 paths in total), and will from now on be used in all optimization formulations.

Next, using path lists $\mathcal{P}(d, 0)$, $d \in \mathcal{D}$, and the resulting path lists $\mathcal{R}(e, d, 0)$, $e \in \mathcal{E}, d \in \mathcal{D}$, we calculate the cheapest link capacity vector sufficient to carry the traffic defined by the vector $\boldsymbol{h}$ in the normal state. This is done by means of the following MIP formulation.

Calculation of link capacities for the normal state

$$\min \sum_{e \in \mathcal{E}} y_e^0 \tag{24a}$$

TABLE 5. Link capacity vectors.

ext. budget	no. of capacity modules: $C(e)$, $e = 1, 2, \ldots, 21$	total
$c(e)$	17, 5, 4, 5, 6, 5, 4, 3, 7, 5, 6, 1, 2, 1, 2, 3, 1, 1, 1, 4, 1	84
$\Delta = 0\%$	14, 2, 4, 4, 5, 5, 6, 2, 6, 5, 6, 2, 2, 1, 3, 5, 2, 2, 2, 5, 1	84
$\Delta = 10\%$	15, 2, 3, 7, 4, 5, 7, 3, 7, 5, 7, 1, 1, 1, 2, 4, 4, 5, 3, 5, 1	92
$\Delta = 20\%$	14, 3, 2, 8, 4, 5, 8, 2, 7, 5, 6, 1, 2, 2, 3, 5, 6, 7, 4, 5, 1	100

$$\sum_{p \in \mathcal{P}(d,0)} x_{dp}^0 \geq h(d), \quad d \in \mathcal{D} \tag{24b}$$

$$\sum_{d \in \mathcal{D}} \sum_{p \in \mathcal{R}(e,d,0)} x_{dp}^0 \leq y_e^0, \quad e \in \mathcal{E} \tag{24c}$$

$$y^0 \geq 0 \text{ and integer}; \quad x^0 \geq 0. \tag{24d}$$

In our traffic protection procedure, the so obtained optimal link capacities y_e^{0*}, $e \in \mathcal{E}$, are denoted by $c(e)$, $e \in \mathcal{E}$, and are assumed to be installed in the existing network. These capacities, shown in the first row of Table 5, determine the value of budget $B = \sum_{e \in \mathcal{E}} c(e)$ and the values of parameters $h(d, s)$ (see (20)) that are used for calculating the extended link capacity vectors C for the increased budget values $B + \Delta$ (for $\Delta = 0\%, 10\%, 20\%$ of B) through solving formulation (19). Note that since all $\xi(e)$ are equal to 1, B is equal to the number of FSO systems installed in the network, and we can assume that the cost of link capacity adjustment is equal to the number of extra FSO systems, i.e., to Δ, which are to be provided. This is because the cost of rearranging the existing FSO systems (there are B of them) is negligible as it only requires moving a number of transceivers, which can be included in the network maintenance costs.

The resulting vectors C are given in Table 5, where column 'total' shows the total number of modules installed on the links.

Once the capacity vector (for a given Δ) is established, the state-dependent demand reduction parameters $F(s)$, $w(s)$, and $T(s)$ are calculated using formulas (20a)-(20c); note that the values of parameter $w(s)$ do not depend on the budget value. The values of these parameters are shown in Fig. 9 for the extra budget $\Delta = 10\%$. In the figure, the states in $\mathcal{S}$ (there

are 75 of them, from $s = 1$ to $s = 75$) are ordered according to non-decreasing $F(s)$. The peak at state $s = 11$ is observed because this state occurs about 10 times more often than any other state.

C. RESULTS OF THE MMF PROCEDURE

Now we proceed to the main part of the numerical study, i.e., application of the MMF algorithm to the PMA network. For that, we will need some new notation: i – the number of iteration in MMFA ($i = 1, 2, \ldots, I$), I – the total number of iterations executed by MMFA, and $t^*(d, s; i)$ – the value of $t^*(d, s)$ assigned to the pair $(d, s) \in \mathcal{Q}$ as the result of iteration no. i. The presented results concern the following measures defined for $s \in \mathcal{S}$ and $d \in \mathcal{D}(s)$:

$$\widehat{h}(d, s; i) = \min\{h(d, s)t^*(d, s; i), h(d)\} \tag{25a}$$

$$H(i) = \frac{\sum_{s \in \mathcal{S}} N(s) \sum_{d \in \mathcal{D}(s)} \widehat{h}(d, s; i)}{\sum_{s \in \mathcal{S}} N(s) \sum_{d \in \mathcal{D}(s)} h(d)} \tag{25b}$$

$$\widehat{\mathcal{D}}(s, \varphi) = \{d \in \mathcal{D}(s) : \frac{\widehat{h}(d, s; I)}{h(d)} \geq \varphi\}, \quad \varphi \in [0\%, 100\%] \tag{25c}$$

$$\widehat{H}(s, \varphi) = \sum_{d \in \widehat{\mathcal{D}}(s,\varphi)} \widehat{h}(d, s; I) \tag{25d}$$

$$\widehat{H}(s) = \widehat{H}(s, \varphi) = \sum_{d \in \widehat{\mathcal{D}}(s)} \widehat{h}(d, s; I). \tag{25e}$$

The quantity $\widehat{h}(d, s; i)$ defined in (25a) measures the traffic realized for a pair $(d, s) \in \mathcal{Q}$ calculated in iteration no. i (the minimum is used because the realized traffic cannot be greater than the nominal traffic $h(d)$). Note that $\widehat{h}(d, s; I)$ is the final value of the traffic realized for (d, s) when MMFA stops. The value of $H(i)$ defined in (25b) expresses the proportion of traffic realized by the MMFA solution after iteration no. i (for all weather states corresponding to the assumed list $\mathcal{S}$ – that is why the weights $N(s)$ are used) with respect to the total traffic calculated for all demand-state pairs (d, s) in $\mathcal{Q}$. Next, equality (25c) defines the set $\widehat{\mathcal{D}}(s, \varphi)$ of those demands d in $\mathcal{D}(s)$ for which the percentage of the traffic volume $\widehat{h}(d, s; I)$ in relation to the nominal traffic volume $h(d)$ is greater than or equal to φ percent. Finally, the quantity $\widehat{H}(s, \varphi)$ defined in (25d) gives the total traffic volume realized for demands $d \in \widehat{\mathcal{D}}(s, \varphi)$, that is the total traffic volume realized in state $s \in \mathcal{S}$ with the percentage φ or more (in relation to the nominal traffic). Note that for the special case of $\varphi = 0\%$, quantity $\widehat{H}(s)$ defined in (25e) specifies the total traffic volume realized in state s.

Table 6 gives the execution details of MMFA, where the consecutive columns express the total computation time (column 'time [s]'), the total number I of iterations (column '#iter.'), and the final value $H(I)$ of the traffic realization measure (column '$H(I)$'). Observe that the extra budget $\Delta = 10\%$ allows to increase the traffic realization by about 8% as compared to the case $\Delta = 0\%$ with no extra budget; adding 10% of B to the extra budget increases the traffic realization by only 1.4%, reaching $H(I) = 0.831$.

Fig. 10 illustrates how the measure $H(i)$, for the three budget values, $\Delta = 0\%, 10\%, 20\%$, increases in the consecutive

TABLE 6. Summary of MMFA.

budget	time [s]	#iter.	$H(I)$
$\Delta = 0\%$	778	1247	0.737
$\Delta = 10\%$	638	1204	0.817
$\Delta = 20\%$	1100	1269	0.831
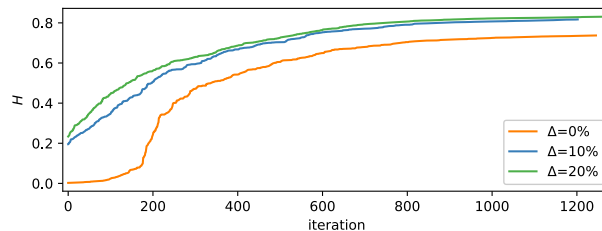
FIGURE 10. Traffic realization measure $H(i)$ in consecutive iterations of MMFA for the three extra budget values.
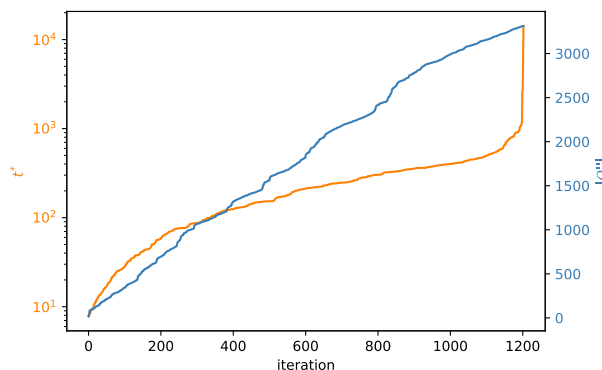
FIGURE 11. t^* and $|\mathcal{Q}''|$ in the consecutive iterations of MMFA ($\Delta = 10\%$).

iterations $i = 1, 2, \ldots, I$. Note that the increase, quite steep in the initial 200 iterations, say, becomes rather flat from iteration no. 600 on.

Next, Fig. 11 illustrates how MMFA increases the value of t^* and the size of $\mathcal{Q}''$ in consecutive iterations for $\Delta = 10\%$. (Recall that MMFA stops when $\mathcal{Q}'' = \mathcal{Q}$, i.e., when the value of $t^*(d, s)$ becomes fixed for all demand-state pairs. In each iteration, the size of $\mathcal{Q}''$ increases by about 2.7 on the average, and all $|\mathcal{Q}| = 3313$ demand-state pairs are finally moved to $\mathcal{Q}''$ in 1204 iterations. On the other hand, the t^* value increases very slowly except for the few (4-5) final iterations where the increase becomes significant (note the logarithmic scale of the t^* axis). This is because of the presence of several severe states in which only a few demands can be realized. Note that for such states the state-dependent demand reduction $T(s)$ factor is small, so it compensates for the large t^* values on the left-hand side of constraint (23d).

In the following, additional results illustrating traffic realization are discussed for three selected states: $s = 68$, $s = 29$, $s = 7$, where the states are numbered as in Fig. 9. The parameters of the selected states, i.e., link availability coefficients $\alpha(e, s)$, the number of demands that can be realized in state s

TABLE 7. Parameters of the three selected states.

state	$\alpha(e,s)$	$|\mathcal{D}(s)|$	$F(s)$	$w(s) = \frac{N(s)}{605}$	$T(s)$
$s=68$	1.00 1.00 1.00 1.00 1.00 1.00 1.00 1.00 1.00 1.00 1.00 1.00 1.00 1.00 0.00 1.00 1.00 1.00 1.00 1.00 1.00	66	0.978	0.018	0.018
$s=29$	0.00 0.29 1.00 1.00 1.00 0.00 0.85 0.00 1.00 0.76 0.95 1.00 0.87 0.59 0.44 0.86 1.00 1.00 1.00 0.31 0.00	55	0.639	0.031	0.020
$s=7$	0.00 0.00 0.00 0.00 0.00 0.00 0.00 0.00 1.00 0.76 0.95 1.00 0.87 0.59 0.00 0.00 0.00 0.00 0.00 0.00 0.00	10	0.216	0.007	0.001

FIGURE 12. Traffic realized by each demand in the final MMFA solution as compared to the nominal demand volume; state $s = 68$; $\Delta = 10\%$.

FIGURE 13. Traffic realized by each demand in the final MMFA solution as compared to the nominal demand volume; state $s = 29$; $\Delta = 10\%$.
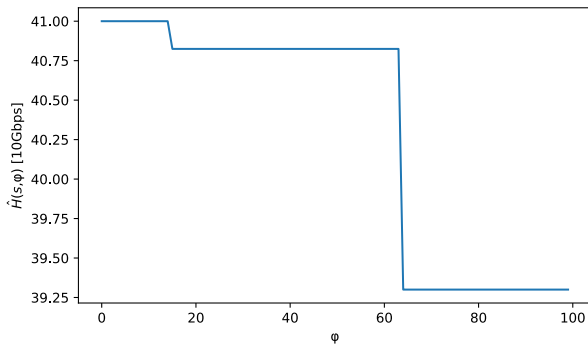
$|\mathcal{D}(s)|$, together with the parameters $F(s)$, $w(s)$, and $T(s)$ are presented in Table 7.

In Figs. 12, 13 and 14, the volume of the realized traffic $\widehat{h}(d, s; I)$ with respect to the nominal traffic volume $h(d)$ is compared for the states $s = 68$, $s = 29$, $s = 7$, respectively, assuming the extra budget $\Delta = 10\%$. In state $s = 68$, one link is unavailable while the others are fully available and $|\mathcal{D}(s)| = 66$. For this state, as shown in Fig. 12, only 7 demands are not fully realized. The state $s = 29$ is more severe: 8 links are fully available, 9 links are partially available, 4 links are not available. In this state, the network is split into two disjoint connected components, and hence not all demands can be realized ($|\mathcal{D}(s)| = 55$). As can be seen in Fig. 13, for such demands we assume $\widehat{h}(d, s, I) = 0$ and $h(d) = 0$. Realization of the remaining demands varies between 20% and 100%. The state $s = 7$ is even more severe: 2 links are fully available, 4 links are partially available, 15 links are not available. In this state, only $|\mathcal{D}(s)| = 10$ demands can be realized (and 6 of them are fully realized).

The next three figures, i.e., Figs. 15, 16, 17, correspond respectively to Figs. 12, 13, 14, and illustrate the quantity $\widehat{H}(s, \varphi)$ defined in (25d). Recall that this quantity expresses the total volume of the traffic realized in state s for those demands whose percentage of realized traffic is equal to at least φ percent, i.e., for those $d \in \mathcal{D}(s)$ for which $\frac{\widehat{h}(d,s,I)}{h(d,s)} 100\% \geq \varphi$. It can be seen that for the least severe of the considered states, i.e., for $s = 68$ with only one link (entirely) unavailable (see Table 7), 41 traffic units (recall that the traffic unit is equal to 10 Gbps), i.e., almost the entire nominal traffic volume (which is equal to 42.9 units), are realized in at least

FIGURE 14. Traffic realized by each demand in the final MMFA solution as compared to the nominal demand volume; state $s = 7$; $\Delta = 10\%$.

20%, and only a slightly smaller volume is realized at the level of at least 60%; moreover, as much as 39.3 units of traffic are realized in 100%. For the second state, i.e., $s = 29$ with 13 affected (mostly partly) links, 11 out of (almost) 18 traffic units are realized in 100%. Finally, although state $s = 7$ is very severe (only 2 links entirely available while as many as 15 links are entirely unavailable), 4.5 out of 5 traffic units are realized in 100%. This may look like a good score but, in fact, it is not since in this state the network becomes disconnected and only 10 demands can be realized, i.e., only 10 node pairs are in the same components.

FIGURE 15. Total traffic realized for the demands with at least φ percent of carried traffic; state $s = 68$; $\Delta = 10\%$.
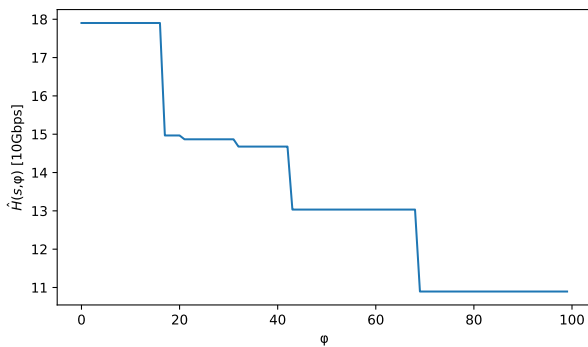

FIGURE 16. Total traffic realized for the demands with at least φ percent of carried traffic; state $s = 29$; $\Delta = 10\%$.
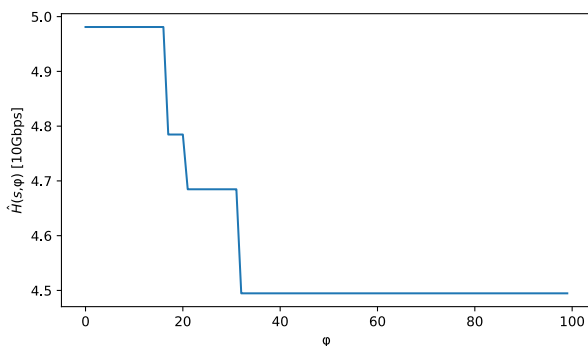

FIGURE 17. Total traffic realized for the demands with at least φ percent of carried traffic; state $s = 7$; $\Delta = 10\%$.

To have a more general insight into how the traffic realization measure $H(s)$ is related to the two basic state characteristics let us examine Fig. 18, which illustrates, for the consecutive states, the dependence on the proportion of the total available link capacity $F(s)$ (20b) and on the state connectivity measured by the number of realizable demands $|\mathcal{D}(s)|$. (The states are ordered according to non-decreasing $F(s)$, like in Fig. 9.) The figure reveals that three groups of states can be distinguished: $s = 1$ to $s = 28$, $s = 29$ to $s = 55$, and $s = 56$ to $s = 75$ (these groups are described in Table 8). For group $\mathcal{S}(3)$, $F(s)$ is high (greater than 0.83)
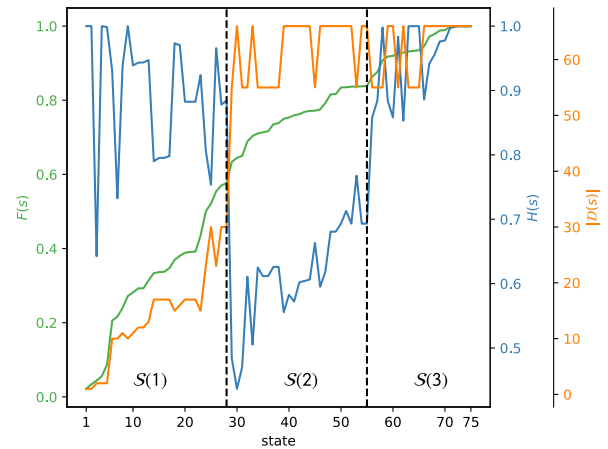

FIGURE 18. $F(s)$, $H(s)$ and $|\mathcal{D}(s)|$; $\Delta = 10\%$.

TABLE 8. Groups of states.

group	states	$F(s)$	$|\mathcal{D}(s)|$	$H(s)$
$\mathcal{S}(1)$	1–28	0.83-1.00	55-66	0.70-1.00
$\mathcal{S}(2)$	29–55	0.56-0.83	55-66	0.45-0.75
$\mathcal{S}(3)$	56–75	0.00-0.56	0-30	0.65-1.00

and the number of demands to be realized $|\mathcal{D}(s)|$ is 55 or 66, and hence $H(s)$ ranges from 0.7 to 1. Next, for group $\mathcal{S}(2)$, $|\mathcal{D}(s)|$ is similar to that for $\mathcal{S}(3)$, while $F(s)$ ranges from 0.56 to 0.83, so the value of $H(s)$ increases and is between 0.45 and 0.75. Finally, group $\mathcal{S}(1)$ consists of the most severe states, for which $F(s)$ is less than 0.55 and $|\mathcal{D}(s)| \leq 30$ so less than half of the demands can be realized (for some of these states only a few demands are realizable). At the same time, $H(s)$ is kept at a higher level than in the case of group $\mathcal{S}(2)$, because the available link capacity serves less than 30 demands.

D. REMARKS

To conclude this section, let us consider some points that have not yet been discussed. First of all, we would like to point out that protecting network traffic from unfavorable weather conditions is not an easy task. Besides a method for translating the current traffic conditions into the corresponding link availability coefficients (see Section III), it requires a pretty complicated mathematical model for optimizing the link capacities and demand traffic flows for each element of the assumed list of states $\mathcal{S}$ (characterized by the precalculated link availability coefficients) that represents all (foggy) states observed in reality.

An important question here is what proportion of the normal traffic volumes (specified by a given traffic matrix) should be realized in a given state $s \in \mathcal{S}$. Our choice is to make this proportion equal to $T(s) = \frac{N(s)}{N}F(s)$ (see (20a)), where $N(s)$ is the number of real (hourly) states that are represented by s, N is the total number of the considered hourly states, and $F(s)$ is the fraction of the total link capacity available in state s with respect to the total maximal link

capacity. In this way we take into account the real duration ($N(s)$ hours) of state s, i.e., its importance when we calculate the total volume of data transmitted in the network during N hours, as well as the current capacity available in s.

Another issue is the max-min fairness principle considered for traffic protection. In our case, we require that the *traffic vector* $(h(d)T(s)t^*(d, s), d \in \mathcal{D}(s), s \in \mathcal{S})$ expressing the traffic to be carried for each demand in each state (in which the demand is realizable) should be *lexicographically maximal*. This means that when this vector is ordered in a non-decreasing manner then it is lexicographically maximal among all feasible traffic vectors ordered in a non-decreasing manner. (Note that in the final solution we assume that the element corresponding to (d, s) in the considered vector is equal to $h(d)$ if $T(s)t^*(d, s) > 1$, but those rare cases do not disrupt the idea of MMF.) This approach is more effective than a frequently used naive fairness approach where the MMFA is executed only once, which is equivalent to maximization of the minimum element of the traffic vector. In fact, such a naive approach would result in the traffic vector $(h(d)T(s)t^1(d, s), d \in \mathcal{D}(s), s \in \mathcal{S})$ where all $t^1(d, s)$ are equal to t^* obtained in the first execution of Step 1, which realizes a substantially smaller amount of traffic than the vector obtained from MMFA.

Another important observation is that for FSO-based metropolitan area networks it would in general be very costly to provide 100% traffic protection. For the considered PMAN instance this issue is illustrated in Table 9 which shows that even with additional budget (which is equal to the number of extra FSO systems) equal to 500%, it is not possible to achieve this goal (recall that the demands that become disconnected are not supposed to be realized). This is because in the states heavily affected by fog there appear links with very low availability coefficients. This observation implies that the links that suffer from fog to a large degree should be realized, if possible, using fiber rather than employing FSO systems [11], [46]. Another possibility to achieve a satisfactory level of traffic throughput during fog is to use combined FSO/RF links [7]. Because RF links are not as susceptible to fog as FSO links (see [79]), their use, combined with flexible routing (achievable due to the mesh network topology) can substantially help in providing a good level of overall traffic throughput, distributed fairly amongst individual demands. Example proposals of hybrid FSO/RF network architectures are presented in [34], [35].

Let us notice that even without the backup fiber/RF links, the mesh topology of networks like PMAN can help to improve the level of fairness in traffic throughput for individual demands. This happens when in a given foggy state there are areas with different fog density. Then, for example, the FSO links in an area clear from fog can be used to transit more traffic between the areas currently affected by fog at the expense of decreasing the intra-area traffic.

Finally, let us mention that MMFA is computationally efficient. The time spent in the consecutive parts of the whole optimization procedure described above are as follows:

TABLE 9. Traffic level $H(I)$ achieved with additional budget Δ.

Δ	$H(I)$
0%	0.737
10%	0.817
20%	0.831
70%	0.853
100%	0.866
200%	0.912
500%	0.964

- path list generation (17): 15–20 s
- link capacity for the normal state (24): < 1 s
- link capacity adjustment (19): 10–15 s
- MMFA: 600–1100 s.

VI. CONCLUSION

In the paper we have proposed a comprehensive approach for traffic protection in FSO networks exposed to adverse weather conditions. The approach consists of two main elements. The first element is a methodology for calculating the degradation ratios characterizing the extent to which the effective bandwidth realized on the FSO links is decreased when the weather is degraded, used for preparing realistic lists of weather states and the corresponding link availability coefficients. Such lists constitute basic input data, on top of the data describing network topology, traffic matrix, existing equipment, etc., for an optimization procedure (which is the second main element of the proposed approach) that protects, in a fair way, the network traffic in the considered states by means of the AFT (affine flow thinning) mechanism. The optimization procedure is pretty advanced and takes into account the FSO systems already provided and also a budget for extra systems required for achieving reasonable protection. An extensive numerical study performed for a Paris Metropolitan Area network shows that the proposed approach works well in terms of both traffic effectiveness of the delivered solutions and of computation time. It also shows that full network traffic protection in highly unfavorable weather conditions can be very costly. Hence, intentional reduction of the assumed traffic throughput (with respect to the nominal traffic matrix) in such conditions is reasonable, especially when this is done in a max-min fair way.

As far as future work is concerned, one of the important issues is to find an efficient, in terms of accuracy, method for estimating the values of the weather parameters (i.e., visibility for fog, and precipitation rate for rain and snow) at arbitrary points within the network area using the values available at the measurement points. Possible approaches for that are for example general function approximation procedures mentioned at the beginning of Section III-C and ad-hoc heuristics as the one described in Section V-A. Both approaches, however, have some intrinsic disadvantages: general estimation methods may neglect the specific character of the functions that characterize the weather conditions in a given area, while the ad-hoc calculations can be unacceptably inaccurate.

It seems that artificial intelligence approaches (like deep learning) is a promising direction of research here.

Another interesting issue is to extend research (and take this opportunity to refine optimization procedures) to the specific types of the FSO systems available on the market.

REFERENCES

[1] M. Uysal, C. Capsoni, Z. Ghassemlooy, A. Boucouvalas, and E. Udvary, *Optical Wireless Communications*. Cham, Switzerland: Springer, 2016.

[2] Z. Gassemlooy, M. Uysal, M. Khalighi, V. Ribeiro, F. Moll, S. Zvanovec, and A. Belmonte, "An overview of optical wireless communications," in *Optical Wireless Communications*, M. Uysal, C. Capsoni, Z. Gassemlooy, and A. B. E. Udvary, Eds. Cham, Switzerland: Springer, 2016, pp. 1–23.

[3] A. G. Shaina, "Comparative analysis of free space optical communication system for various optical transmission windows under adverse weather conditions," *Procedia Comput. Sci.*, vol. 89, pp. 99–106, Jan. 2016.

[4] A. Gupta, S. Bakshi, and M. Chaudhary, "Improving performance of free space optics link using array of receivers in terrible weather conditions of plain and hilly areas," *Int. J. Adv. Res. Artif. Intell.*, vol. 5, no. 3, p. 3, 2016.

[5] E. Leitgeb, T. Plank, M. S. Awan, P. Brandl, W. Popoola, Z. Ghassemlooy, F. Ozek, and M. Wittig, "Analysis and evaluation of optimum wavelengths for free-space optical transceivers," in *Proc. 12th Int. Conf. Transparent Opt. Netw.*, Jun. 2010, pp. 1–7.

[6] J. Rak and D. Hutchison, *Guide to Disaster-Resilient Communication Networks*. Cham, Switzerland: Springer, 2020.

[7] M. A. Khalighi and M. Uysal, "Survey on free space optical communication: A communication theory perspective," *IEEE Commun. Surveys Tuts.*, vol. 16, no. 4, pp. 2231–2258, Jun. 2014.

[8] E. Leitgeb and T. Plank, "Combination of free space optics (FSO) and RF for different wireless application scenarios," in *Proc. 9th Eur. Conf. Antennas Propag. (EuCAP)*, Lisbon, Portugal, Apr. 2015, pp. 1–4.

[9] V. Chan, "Free-space optical communications," *J. Lightw. Technol.*, vol. 24, no. 12, pp. 4750–4762, Dec. 2006.

[10] M. Tornatore, J. André, P. Babarczi, T. Braun, E. Følstad, P. Heegaard, A. Hmaity, M. Furdek, L. Jorge, W. Kmiecik, C. Mas-Machuca, L. Martins, C. Medeiros, F. Musumeci, A. Pašić, J. Rak, S. Simpson, R. Travanca, and A. Voyiatzis, "A survey on network resiliency methodologies against weather-based disruptions," in *Proc. 8th Int. Workshop Resilient Netw. Design Model. (RNDM)*, vol. 8, Sep. 2016, pp. 23–34.

[11] Y. Li, N. Pappas, V. Angelakis, M. Pióro, and D. Yuan, "Optimization of free space optical wireless network for cellular backhauling," *IEEE J. Sel. Areas Commun.*, vol. 33, no. 9, pp. 1841–1854, Sep. 2015.

[12] Y. Li, N. Pappas, V. Angelakis, M. Pióro, and D. Yuan, "On the resilient network design of free-space optical wireless network for cellular backhauling," in *Optical Wireless Communications*. Cham, Switzerland: Springer, 2016, pp. 485–510.

[13] I. K. Son and S. Mao, "A survey of free space optical networks," *Digit. Commun. Netw.*, vol. 3, no. 2, pp. 67–77, 2017.

[14] V. K. Mogadala, S. R. Gottapu, and B. P. Chapa, "Wireless optical based backhaul communication for 5G cellular systems," in *Proc. Int. Conf. Recent Innov. Electr., Electron. Commun. Eng. (ICRIEECE)*, Jul. 2018, pp. 718–721.

[15] Z. Gu, J. Zhang, and Y. Ji, "Topology optimization for FSO-based fronthaul/backhaul in 5G+ wireless networks," in *Proc. IEEE Int. Conf. Commun. Workshops (ICC Workshops)*, May 2018, pp. 1–6.

[16] Z. Gu, J. Zhang, Y. Ji, L. Bai, and X. Sun, "Network topology reconfiguration for FSO-based fronthaul/backhaul in 5G+ wireless networks," *IEEE Access*, vol. 6, pp. 69426–69437, 2018.

[17] M. Alzenad, M. Z. Shakir, H. Yanikomeroglu, and M.-S. Alouini, "FSO-based vertical backhaul/fronthaul framework for 5G+ wireless networks," *IEEE Commun. Mag.*, vol. 56, no. 1, pp. 218–224, Jan. 2018.

[18] S. Song, Y. Liu, Q. Song, and L. Guo, "Relay selection and link scheduling in cooperative free-space optical backhauling of 5G small cells," in *Proc. IEEE/CIC Int. Conf. Commun. China (ICCC)*, Oct. 2017, pp. 1–6.

[19] *Free Space Optics (FSO) and Visible Light Communication (VLC)/Light Fidelity (Li-Fi) Market With COVID-19 Impact Analysis by Component (LED, Photodetector, Microcontroller, Software), Transmission Type, Application, Geography—Global Forecast to 2025*. Accessed: Jun. 16, 2021. [Online]. Available: https://www.marketsandmarkets.com/Market-Reports/visible-light-communication-market-946.html

[20] *LightePointe AireLink 80 10 Gbps 70/80 GHz Radios*. Accessed: Jun. 9, 2021. [Online]. Available: https://www.lightpointe.com/10-gbps-radios

[21] *Wireless Excellence-LTD*. Accessed: Aug. 17, 2021. [Online]. Available: https://www.cablefree.net/

[22] H. Ivanov, E. Leitgeb, D. Kraus, F. Marzano, A. Jurado-Navas, S. Dorenbos, and R. Perez-Jimenez, "Free space optics system reliability in the presence of weather-induced disruptions," in *Guide to Disaster-Resilient Communication Networks*, J. Rak and D. Hutchison, Eds. Cham, Switzerland: Springer, 2020.

[23] (2016). D. Meissler. *DLR Researchers Set World Record in Free-Space Optical Communications*. [Online]. Available: https://www.parabolicarc.com/2016/11/05/dlr-researchers-set-world-record-freespace-optical-communications/

[24] A. K. Majumdar, "Free-space laser communication performance in the atmospheric channel," *J. Opt. Fiber Commun. Res.*, vol. 2, no. 4, pp. 345–396, Oct. 2005.

[25] I. Djordjevic, W. Ryan, and B. Vasic, "Channel coding for optical channels," in *Coding for Optical Channels*. Springer, 2010, pp. 123–178.

[26] A. Majumdar, *Advanced Free Space Optics (FSO): A systems approach*. New York, NY, USA: Springer, 2015.

[27] A. Vavoulas, H. G. Sandalidis, and D. Varoutas, "Weather effects on FSO network connectivity," *IEEE/OSA J. Opt. Commun. Netw.*, vol. 4, no. 10, pp. 734–740, Oct. 2012.

[28] L. Andrews and R. Phillips, *Laser Beam Propagation Trough Random Media*, 2nd ed. Bellingham, WA, USA: SPIE, 2005.

[29] S. S. Muhammad, B. Flecker, E. Leitgeb, and M. Gebhart, "Characterization of fog attenuations in terrestrial free space optical links," *Optical Eng.*, vol. 46, no. 6, pp. 53–56, 2007.

[30] E. Leitgeb, M. Gebhart, P. Fasser, J. Bregenzer, and J. Tanczos, "Impact of atmospheric effects in free-space optics transmission systems," *Proc. SPIE*, vol. 4976, pp. 86–97, Apr. 2003.

[31] F. P. Guiomar, A. Lorences-Riesgo, D. Ranzal, F. Rocco, A. N. Sousa, A. Carena, A. L. Teixeira, M. C. R. Medeiros, and P. P. Monteiro, "High-capacity and rain resilient free-space optics link enabled by time-adaptive probabilistic shaping," in *Proc. 45th Eur. Conf. Opt. Commun. (ECOC)*, 2019, pp. 1–4. [Online]. Available: https://ieeexplore.ieee.org/abstract/document/9125592, doi: 10.1049/cp.2019.0864.

[32] *CableFree.net: FSO: Fog & Attenuation*. Accessed: Aug. 16, 2021. [Online]. Available: https://www.cablefree.net/wirelesstechnology/free-space-optics/fso-fog-% attenuation

[33] I. I. Kim, B. McArthur, and E. J. Korevaar, "Comparison of laser beam propagation at 785 nm and 1550 nm in fog and haze for optical wireless communications," *Proc. SPIE*, vol. 4214, pp. 26–37, Feb. 2001.

[34] L. B. Stotts, L. C. Andrews, P. C. Cherry, J. J. Foshee, P. J. Kolodzy, W. K. McIntire, M. Northcott, R. L. Phillips, H. A. Pike, B. Stadler, and D. W. Young, "Hybrid optical RF airborne communications," *Proc. IEEE*, vol. 97, no. 6, pp. 1109–1127, May 2009.

[35] F. Nadeem, V. Kvicera, M. S. Awan, E. Leitgeb, S. S. Muhammad, and G. Kandus, "Weather effects on hybrid FSO/RF communication link," *IEEE J. Sel. Areas Commun.*, vol. 27, no. 9, pp. 1687–1697, Dec. 2009.

[36] D. O. Caplan, "Laser communication transmitter and receiver design," *J. Opt. Fiber Commun. Rep.*, vol. 4, nos. 4–5, pp. 225–362, Sep. 2007.

[37] H. Ivanov, T. Plank, E. Leitgeb, L. Mustafa, and E. Cerncic, "Estimation of Mie scattering influence for the FSO channel under artificially simulated fog conditions," *Proc. SPIE* vol. 10787, Sep. 2018, Art. no. 107870R.

[38] R. Bruzgiene, L. Narbutaite, T. Adomkus, P. Pocta, P. Brida, J. Machaj, E. Leitgeb, P. Pezzei, H. Ivanov, N. Kunicina, A. Zabasta, J. Caiko, and A. Patlins, "Quality-driven schemes enhancing resilience of wireless networks under weather disruptions," in *Guide to Disaster-Resilient Communication Networks*, J. Rak and D. Hutchison, Eds. Cham, Switzerland: Springer, 2020.

[39] C. E. Shannon, "A mathematical theory of communication," *Bell Syst. Tech. J.*, vol. 27, no. 3, pp. 379–423, Jul./Oct. 1948.

[40] A. Chaaban and S. Hranilovic, "Capacity of optical wireless communication channels," *Philos. Trans. Roy. Soc. A*, vol. 378, Apr. 2020, Art. no. 20190184.

[41] A. A. Farid and S. Hranilovic, "Capacity bounds for wireless optical intensity channels with Gaussian noise," *IEEE Trans. Inf. Theory*, vol. 56, no. 12, pp. 6066–6077, Dec. 2010.

[42] A. Lapidoth, S. M. Moser, and M. A. Wigger, "On the capacity of free-space optical intensity channels," *IEEE Trans. Inf. Theory*, vol. 55, no. 10, pp. 4449–4461, Oct. 2009.

[43] J. M. Garrido-Balsells, A. Jurado-Navas, J. F. Paris, M. Castillo-Vazquez, and A. Puerta-Notario, "On the capacity of M distributed atmospheric optical channels," *Opt. Lett.*, vol. 39, no. 3, p. 653, 2014.

[44] M. Shehaj, I. Kalesnikau, D. Nace, M. Pióro, and E. Qafzezi, "Modeling transmission degradation on FSO links caused by weather phenomena for WMN optimization," in *Proc. 11th Int. Workshop Resilient Netw. Design Model. (RNDM)*, Oct. 2019, pp. 1–7.

[45] D. Nace, M. Pióro, M. Poss, F. D'Andreagiovanni, I. Kalesnikau, M. Shehaj, and A. Tomaszewski, "An optimization model for robust FSO network dimensioning," *Opt. Switching Netw.*, vol. 32, pp. 25–40, Apr. 2019.

[46] M. Shehaj, D. Nace, I. Kalesnikau, and M. Pióro, "Link dimensioning of hybrid FSO/fiber networks resilient to adverse weather conditions," *Comput. Netw.*, vol. 161, pp. 1–13, Oct. 2019.

[47] M. Shehaj, "Robust dimensioning of wireless optical networks with multiple partial link failures," Ph.D. dissertation, Lab. Heudiasyc, Université de Technologie de Compiègne, HeuDiaSyC, UMR CNRS 7253, Compiègne, France, Feb. 2020.

[48] R. Wessäly, *Dimensioning Survivable Capacitated Networks*. Göttingen, Germany: Cuvillier Verlag Gottingen, 2000.

[49] W. D. Grover, *Mesh-SASED Survivable Networks: Options and Strategies for Optical, MPLS, SONET and ATM Networking*. Upper Saddle River, NJ, USA: Prentice-Hall, 2003.

[50] M. Pióro and D. Medhi, *Flow and Capacity Design in Communication and Computer Networks*. San Mateo, CA, USA: Morgan-Kaufmann, 2004.

[51] J. Strand, A. L. Chiu, and R. Tkach, "Issues for routing in the optical layer," *IEEE Commun. Mag.*, vol. 39, no. 2, pp. 81–87, Feb. 2001.

[52] S. Orlowski and M. Pióro, "Complexity of column generation in network design with path-based survivability mechanisms," *Networks*, vol. 59, no. 1, pp. 132–147, Jan. 2012.

[53] P. Nilsson, M. Pióro, and Z. Dziong, "Link protection within an existing backbone network," in *Proc. Int. Netw. Opt. Conf. (INOC)*, Paris-Evry, France, 2003, pp. 435–440.

[54] W. Ogryczak, M. Pióro, and A. Tomaszewski, "Telecommunications network design and max-min optimization problem," *Telecommun. Inf. Technol.*, vol. 3, pp. 43–56, 2005.

[55] G. Classen, D. Coudert, A. Koster, and N. Nepomuceno, "A chance-constrained model and cutting planes for fixed broadband wireless networks," in *Proc. Int. Conf. Netw. Optim.*, 2011, pp. 37–42.

[56] D. Nace and M. Pióro, "Max-min fairness and its applications to routing and load-balancing in communication networks: A tutorial," *IEEE Commun. Surveys Tuts.*, vol. 10, no. 4, pp. 5–17, Oct. 2008.

[57] M. Pióro, Y. Fouquet, D. Nace, and M. Poss, "Optimizing flow thinning protection in multicommodity networks with variable link capacity," *Oper. Res.*, vol. 64, no. 2, pp. 273–289, Apr. 2016.

[58] A. M. C. A. Koster, A. Zymolka, M. Jäger, and R. Hülsermann, "Demand-wise shared protection for meshed optical networks," *J. Netw. Syst. Manage.*, vol. 13, no. 1, pp. 35–55, Mar. 2005.

[59] R. Wessäly, S. Orlowski, A. Zymolka, A. Koster, and C. Gruber, "Demand-wise shared protection revisited: A new model for survivable network design," in *Proc. 2nd Int. Netw. Optim. Conf. (INOC)*, 2005, pp. 100–105.

[60] A. Tomaszewski, M. Pióro, and M. Z. otkiewicz, "On the complexity of resilient network design," *Netw., Int. J.*, vol. 55, no. 2, pp. 109–118, 2010.

[61] I. Shinko, Y. Foquet, and D. Nace, "A study on a distributed rerouting scheme," in *Proc. 27th Int. Conf. Adv. Inf. Netw. Appl. Workshops*, Spain, Barcelona, Mar. 2013, pp. 1461–1466.

[62] M. Poss and C. Raack, *Affine Recourse for the Robust Network Design Problem: Between Static and Dynamic Routing, Network Optimization*, S. V. J. Pahl and T. Reiners, Ed. Berlin, Germany: Springer, 2011, pp. 150–155.

[63] M. Pioro, I. Kalesnikau, and M. Poss, "An optimization model for affine flow thinning—A traffic protection mechanism for FSO networks," in *Proc. 9th Int. Workshop Resilient Netw. Design Model. (RNDM)*, Alghero, Italy, Sep. 2017, pp. 1–7.

[64] M. Pióro, I. Kalesnikau, and M. Poss, "Path generation for affine flow thinning," *Electronic Notes Discrete Math.*, vol. 64, pp. 355–364, Feb. 2018.

[65] M. Pióro, I. Kalesnikau, and M. Poss, "An optimization model for quadratic flow thinning—A traffic protection mechanism for FSO networks," *Opt. Switching Netw.*, vol. 31, pp. 168–182, Jan. 2019.

[66] M. Pióro, E. Fitzgerald, I. Kalesnikau, D. Nace, and J. Rak, "Optimization of wireless networks for resilience to adverse weather conditions," in *Guide to Disaster-Resilient Communication Networks*, J. Rak and D. Hutchison, Eds. Springer, 2020, pp. 523–556.

[67] S. Milner, C. Davis, H. Zhang, and J. Llorca, "Nature-inspired self-organization, control, and optimization in heterogeneous wireless networks," *IEEE Trans. Mobile Comput.*, vol. 11, no. 7, pp. 1207–1222, Jul. 2012.

[68] Z. Ghassemlooy, W. Popoola, and S. Rajbhandari, *Optical Wireless Communications: System and Channel Modelling With MATLAB*, 2nd ed. Boca Raton, FL, USA: CRC Press, 2018.

[69] Z. Htay, N. Mohan, M. M. Abadi, Z. Ghassemlooy, A. Burton, and S. Zvanovec, "Implementation and evaluation of a 10 Gbps real-time FSO link," in *Proc. 3rd West Asian Symp. Opt. Millimeter-Wave Wireless Commun. (WASOWC)*, Nov. 2020, pp. 1–7.

[70] K. S. Neha, "Role of modulators in free space optical communication," *Int. J. Eng. Technol., Manage. Appl. Sci.*, vol. 4, no. 9, pp. 92–96, 2016.

[71] H. Ivanov, E. Leitgeb, T. Plank, P. Bekhrad, and T. Mitsev, "Link budget optimization of free space optical systems in relation to the beam diverging angle," in *Proc. 13th Int. Conf. Telecommun. (ConTEL)*, Graz, Austria, Jul. 2015, pp. 1–5.

[72] T. Y. Elganimi, "Studying the BER performance, power- and bandwidth-efficiency for FSO communication systems under various modulation schemes," in *Proc. IEEE Jordan Conf. Appl. Electr. Eng. Comput. Technol. (AEECT)*, Dec. 2013, pp. 1–6.

[73] L. Andrews, R. Phillips, and C. Hopen, *Laser Beam Scintillation With Applications*. Bellingham, WA, USA: SPIE, 2001.

[74] E. Jones, T. Oliphant, and P. Peterson. (2001). *SciPy: Open Source Scientific Tools for Python*. [Online]. Available: https://www.scipy.org/

[75] E. Jones, T. Oliphant, and P. Peterson. (2001). *SciPy: Open Source Scientific Tools for Python, Interpolate.Griddata*. [Online]. Available: https://docs.scipy.org/doc/scipy/reference/generated/scipy.interpolate.griddata.html

[76] R. Nebuloni and C. Capsoni, "Effaects of Adverse Weather on free space optics," in *Optical Wireless Communications*, M. Uysal, C. Capsoni, Z. Gassemlooy, and A. B. E. Udvary, Eds. Springer, 2016, pp. 47–68.

[77] A. Bokwa, M. J. Hajto, J. P. Walawender, and M. Szymanowski, "Influence of diversified relief on the urban heat island in the city of Kraków, Poland," *Theor. Appl. Climatol.*, vol. 122, nos. 1–2, pp. 365–382, Oct. 2015.

[78] I. Kalesnikau, M. Pióro, M. Poss, D. Nace, and A. Tomaszewski, "A robust optimization model for affine/quadratic flow thinning—A traffic protection mechanism for networks with variable link capacity," *Networks*, vol. 75, no. 4, pp. 420–437, Jun. 2019.

[79] B. Makki, T. Svensson, T. Eriksson, and M.-S. Alouini, "On the performance of RF-FSO links with and without hybrid ARQ," *IEEE Trans. Wireless Commun.*, vol. 15, no. 7, pp. 4928–4943, Jul. 2016.

ILYA KALESNIKAU received the B.S. and M.S. degrees in telecommunications from Warsaw University of Technology, Poland, in 2015 and 2017, respectively, where he is currently pursuing the Ph.D. degree with the Faculty of Electronics and Information Technology, Institute of Telecommunications. His research interests include modeling and optimization of telecommunication and computer networks, operational research, and combinatorial optimization.

MICHAŁ PIÓRO (Senior Member, IEEE) received the Ph.D. degree in telecommunications and the D.Sc. (Habilitation) degree from Warsaw University of Technology, Poland, in 1979 and 1990, respectively. He is currently a Professor with the Faculty of Electronics and Information Technology, Institute of Telecommunications, Warsaw University of Technology. He received a Polish State Professorship—the highest scientific title in Poland, in 2002. From 2000 to 2018, he was a Professor with the Department of Electrical and Information Technology, Lund University, Sweden. Since 2021, he has been a part-time Professor with Gdańsk University of Technology, Poland. He is the author of the recognized monograph *Routing, Flow, and Capacity Design in Communication and Computer Networks* (Morgan-Kaufmann Publishers, Elsevier, 2004) in the area, and more than 200 technical articles presented in telecommunications and operations research journals, and conference proceedings. He has led many research projects in networking for telecom industry in Poland and Sweden, and has been deeply involved in international research through participation in EC projects (FP6, FP7, Celtic, and COST) and ITU projects. His research interests include modeling, optimization, and performance evaluation of communication and computer networks.

JACEK RAK (Senior Member, IEEE) received the M.Sc., Ph.D., and D.Sc. (Habilitation) degrees from Gdańsk University of Technology, Gdańsk, Poland, in 2003, 2009, and 2016, respectively.

From 2016 to 2020, he was leading the COST CA15127 Action *Resilient Communication Services Protecting End-user Applications From Disaster-Based Failures* (RECODIS) involving over 170 members from 31 countries. He is currently an Associate Professor and the Head of the Department of Computer Communications, Gdańsk University of Technology. He has authored over 100 publications, including the monograph *Resilient Routing in Communication Networks* (Springer, 2015). His research interests include the resilience of communication networks and networked systems.

Prof. Rak is a member of the Editorial Board of *Optical Switching and Networking* (Elsevier) and the Founder of the Workshop on Resilient Networks Design and Modeling (RNDM). He has also served as a TPC member for numerous conferences and journals. He has been the General Chair of ITS-T'17 and MMM-ACNS'17, the General Co-Chair of NETWORKS'16, the TPC Chair of ONDM'17, and the TPC Co-chair of IFIP Networking'19.

EMMA FITZGERALD (Member, IEEE) received the bachelor's degree in computer engineering and mathematics and the Ph.D. degree in vehicular ad-hoc networks from The University of Sydney, Australia, in 2008 and 2013, respectively. She joined the Department of Electrical and Information Technology, Lund University, as a Postdoctoral Researcher, in 2014, for a period of two years, after which she has continued there and currently an Associate Professor. Her research interests include cooperative networking and network performance, with particular focus on the Internet of Things.

HRISTO IVANOV received the B.Sc. and M.Sc. degrees from the Technical University of Sofia, Sofia, Bulgaria, in 2011 and 2013, respectively, and the Dr.Techn. (Ph.D.) degree (Hons.) in optical wireless communications from Graz University of Technology, Graz, Austria, in 2020.

He is currently a full-time Project and Teaching Assistant with the Institute of Microwave and Photonic Engineering, Graz University of Technology. He had various international research stays and collaborations in Europe as well as North America, including half a year research and teaching with McMaster University, Hamilton, ON, Canada, in 2015. He has been involved in European Space Agency (ESA), COST actions (COST CA15127 RECODIS and CA16220), OeAD WTZ and national projects. He is also part of the NEWFOCUS Project (COST CA19111). He is the author or coauthor of more than 20 scientific articles and conference contributions. His research interests include free space optics (FSO) technology with strong expertise in terrestrial, near- and deep-space optical communication.
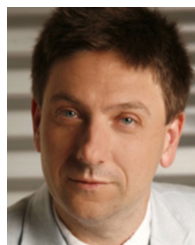
ERICH LEITGEB (Member, IEEE) was born in Fürstenfeld, Austria, in 1964. He received the master's and Ph.D. (Hons.) degrees from TU Graz, in 1994 and 1999, respectively.

Since 2000, he has been the Project Leader of international research projects in the field of optical communications. He submitted his research work for an Associate Professor, in 2003. Since 2011, he has been a Professor of optical communications and wireless applications with the Institute of Microwave and Photonic Engineering, TU Graz. He is giving lectures in optical communications engineering, antennas and wave propagation and microwaves. He is involved in several international co-operations (including research stays, teaching mobilities, and guest's hosting). He is the author/coauthor of seven book chapters, 50 journal publications, and 150 reviewed conference papers.

Dr. Leitgeb is a member of SPIE, OSA, and WCA, a Representative of EurAAP, and Austrian Delegate of URSI Commission B.

● ● ●